

Cite this: *Environ. Sci.: Nano*, 2026, 13, 427

Inflammatory and oxidative responses to PET nanoplastics in the leech *Hirudo verbana*: a comparative analysis of acute and chronic exposure

C. Bon,^a L. Pulze,^{ab} S. Amoroso,^a E. Bertola,^a M. Barbaro,^a D. Tessaro,^c N. Baranzini^{*ab} and A. Grimaldi^{id}^{*ab}

Nanoplastics (NPs) are emerging environmental contaminants with the potential to induce cellular stress and immune dysregulation in aquatic organisms. In this study, the freshwater leech *Hirudo verbana* was used as a non-conventional invertebrate model to investigate the effects of acute (24–72 hours) and chronic (1 week–1 month) exposure to polyethylene terephthalate nanoplastics (PET NPs). A multidisciplinary approach combining microscopy, histology, immunocytochemistry, and qPCR was employed to evaluate PET NP uptake and biological responses. PET NPs were internalised in leech tissues and detected in macrophage-like cells. Both exposure regimes triggered a time- and dose-dependent inflammatory response, characterised by macrophage-like cell recruitment, angiogenic remodelling, and upregulation of the pro-inflammatory marker *HmAlf-1*. Endothelial activation was confirmed by increased CD31 expression and neovascularisation. Furthermore, oxidative stress was evidenced by altered expression of glutathione S-transferase (*GST*) and superoxide dismutase (*SOD*) genes. Overall, PET NPs induced conserved immune and stress responses in *H. verbana*, supporting its relevance as an alternative model for nanoplastic ecotoxicology. These findings contribute to our understanding of NP-induced pathophysiology and reinforce the need for further investigation into the ecological impact of plastic pollution on freshwater invertebrates.

Received 8th August 2025,
Accepted 7th November 2025

DOI: 10.1039/d5en00733j

rsc.li/es-nano

Environmental significance

Our findings underscore the ecological relevance of PET nanoplastics as emerging contaminants in freshwater systems. The observed immune activation, oxidative stress, and vascular remodelling in *H. verbana* highlight conserved biological responses to nanoparticle exposure and point to a limited capacity for long-term physiological compensation under chronic stress. These results emphasise the potential for PET nanoplastics to disrupt immune and tissue homeostasis in aquatic invertebrates, reinforcing the need for their inclusion in environmental risk assessments and regulation of plastic-derived nanomaterials.

Introduction

The increasing production and widespread use of plastic materials have led to the pervasive presence of micro- and nanoplastics (MPs and NPs) in aquatic ecosystems, raising growing concern for environmental and public health. Once released, plastic debris undergoes progressive weathering and fragmentation, leading to the generation of these smaller and

more reactive particles whose environmental fate is difficult to predict, as it depends on a combination of physicochemical properties and local ecological conditions.^{1,2} Notably, it is worth noting that, beyond their intrinsic persistence, an additional factor that further complicates the environmental fate of these particles is their strict connection with climate change. The production and degradation of plastics contribute significantly to greenhouse gas emissions, while climate change in turn amplifies their dispersion, fragmentation, and ecological impacts through extreme weather events, altered hydrological cycles, and ocean warming.³ Based on these perspectives, this interaction highlights the interconnected risks for environmental, animal, and human health, broadening the context of nanoplastic pollution beyond the local ecological impacts.

^a Department of Biotechnology and Life Sciences, University of Insubria, 3 J.H. Dunant Street, 21100, Varese, Italy. E-mail: nicolo.baranzini@uninsubria.it, annalisa.grimaldi@uninsubria.it

^b Italian Leech Farm (ILFARM), S.r.l, via Guicciardini 14, Varese, Italy

^c Department of Chemistry, Materials and Chemical Engineering “Giulio Natta”, Polytechnic University, Milano, Italy



Polyethylene terephthalate (PET) was selected for this study because, unlike other widely used plastics such as polystyrene (PS) and polypropylene (PP), it possesses a unique combination of physicochemical properties that influence its environmental behaviour and biological interactions. Specifically, PET's molecular structure confers high stability and resistance to biodegradation, resulting in its persistent accumulation in freshwater ecosystems. Its relatively hydrophilic surface and high surface energy promote extensive interactions with biological membranes and macromolecules, potentially enhancing cellular uptake and cytotoxic effects at the nanoscale. While PP and PS are also ecologically relevant plastic pollutants, PET's distinctive chemical composition and reactivity make it a particularly suitable candidate for studying the mechanisms of nanoplastic toxicity and tissue-level impacts.^{4,5} Indeed, once released into the environment, PET NPs can be ingested or absorbed by aquatic fauna, crossing epithelial barriers and interacting with biological tissues at the cellular and molecular levels.

Despite their ecological relevance, the effects of nanoplastics on aquatic invertebrates remain largely underexplored. Traditional models such as *Mytilus galloprovincialis*, *Eisenia fetida*, and *Daphnia magna* have proven valuable for investigating sublethal effects of environmental stressors, including oxidative damage, immune modulation, and tissue remodelling.^{6–8} Among alternative invertebrate models, the medicinal leech *Hirudo verbana* has emerged as a promising candidate due to its well-characterised innate immune system, the accessibility of its mucosal and vascular tissues, and the evolutionary conservation of key stress-response pathways.

Unlike classical invertebrate models such as *Drosophila melanogaster* or *Caenorhabditis elegans*, *H. verbana* possesses a closed circulatory system, circulating immune cells, and vascular-like structures that closely resemble those of vertebrates.^{9,10} These features enable biologically relevant investigations into inflammation, oxidative stress, and vascular remodelling. Its immune system includes conserved elements analogous to those in vertebrates, as demonstrated by transcriptomic analyses revealing high homology between leech innate immune genes and their mammalian counterparts.¹¹ Previous studies have shown that *H. verbana* responds to environmental pollutants, including polypropylene (PP) nanoplastics and per- and polyfluoroalkyl substances (PFAS), with dose-dependent changes in gene expression, immune activation, and oxidative stress.^{12,13} In addition, the leech's botryoidal tissue, a multifunctional hematopoietic and vascular structure, plays a central role in immune surveillance, inflammation, and detoxification. Specifically, it serves as the primary hematopoietic niche by producing and mobilising immune cells, contributes to xenobiotic clearance and sequestration of toxicants, and undergoes angiogenic remodelling to restore tissue homeostasis during stress conditions. Owing to this combination of immune, vascular, and detoxification functions, the botryoidal tissue represents a key target of nanoplastic-induced toxicity, providing a unique framework for studying the interplay between immune

responses, angiogenesis, and tissue repair in *H. verbana*.¹⁴ In our previous work, we demonstrated that both short-term (1 and 6 hours) and long-term (1 week, 1 and 2 months) exposure to a mixture of PP MPs and NPs induced inflammatory responses in *H. verbana*, including activation of immune markers and oxidative stress pathways.¹² These findings highlighted the capacity of nanoplastics to interfere with fundamental biological processes, even at early stages of exposure.

For these reasons, here we extend this investigation by evaluating the effects of both acute (24 hours) and chronic (30 days) exposure to PET NPs in *H. verbana*. The concentrations of plastics employed not only mimic those environmentally measured in freshwater systems,¹ but are also comparable to those recently tested in several ecotoxicological assessments conducted on freshwater organisms, such as *D. magna* and *Thamnocephalus platyurus*.¹⁵ However, although several global reviews highlight marked spatial and temporal variability, with contamination levels strongly influenced by anthropogenic activities, it has been observed that in these environments, PET is one of the most predominant contributors to plastic pollution.¹⁶ In addition, from an ecological standpoint, this range can be considered representative, encompassing both concentrations that may induce sub-lethal physiological or behavioural alterations typical of moderately impacted freshwater systems, and worst-case scenarios, in which higher quantities of PET NPs have been measured, such as hotspots in proximity to wastewater discharge points.¹⁷ Using a multidisciplinary approach that combines histological, molecular, and immunological analyses, we aimed to: (i) assess the uptake and tissue distribution of PET NPs; (ii) evaluate the activation of innate immune responses and oxidative stress pathways; and (iii) explore the involvement of angiogenesis and botryoidal tissue remodelling in the organism's response. By elucidating these integrated responses, we provide new insights into the biological effects of PET nanoplastics in freshwater invertebrates and further support the use of *H. verbana* as a sensitive and ecologically relevant model for environmental toxicology and risk assessment.

Materials and methods

Preparation and fluorescent labelling of PET nanoplastics

Polyethylene terephthalate (PET) nanoparticles (NPs) were kindly provided by Dr. Davide Tessaro (Politecnico di Milano). PET microplastics were first dissolved in hexafluoroisopropanol (HFIP) and subsequently added to ten volumes of ultrapure water to induce precipitation and nanoparticle formation. Larger aggregates were removed by filtration, and residual solvent was eliminated *via* rotary evaporation. The resulting PET NPs were labelled with Nile Red dye (Merck Life Science Srl, Italy; excitation/emission: ~549/628 nm), known for its hydrophobic affinity, either by direct incorporation into the HFIP-polymer solution or by copolymerization using a carbazole-based comonomer, as previously described.¹⁸ The final NP concentration was determined by weighing after centrifugation and vacuum drying.



Nanoplastic characterization

The size distribution and morphology of PET NPs were assessed by Dynamic Light Scattering (DLS) and Transmission Electron Microscopy (TEM). DLS confirmed the hydrodynamic diameter of particles. For TEM, 100 μL of NP solution was deposited onto carbon-coated Formvar copper grids (300 mesh, Sigma-Aldrich, Milan, Italy) and examined with a JEOL1400Plus transmission electron microscope (Centro di Ricerca e Trasferimento Tecnologico – CRIETT, University of Insubria – instrument code MIC01). Data were recorded with a MORADA digital camera system (Olympus, Tokyo, Japan). Fluorescence properties were analysed using a Nikon Digital Sight DS-SM (Tokyo, Japan) equipped with 550/570 nm (Cy3) or 560/620 nm filters for Nile Red detection. Digital images were acquired using a DS-5M-L1 digital camera (Nikon, Tokyo, Japan). In addition, further DLS analyses on PET nanoparticles, identical to those used in this study (the same synthesis and properties, without the fluorescent probe), were performed to assess the stability of the nanoparticle suspensions. Measurements were carried out by comparing freshly prepared suspensions with samples stored in water at 4 °C for 9 months.

Animal husbandry and experimental design

The use of the leech *H. verbana* is not among the animals protected under Directive 2010/63/EU, which governs the use of animals in scientific research, nor is it listed in Legislative Decree no. 26, of 4 March 2014, “Implementing Directive 2010/63/EU on the protection of animals used for scientific purposes”, published in the Italian Official Journal on 14 March 2014. However, its use has been approved by the Animal Welfare Body (OPBA) at the University of Insubria, and it complies with the commonly accepted 3Rs.

Adult specimens of *Hirudo verbana* (Annelida, Hirudinea), provided by ILFARM S.r.l. (Varese, Italy), were maintained in aerated freshwater tanks (NaCl 1.5 g L^{-1}) at 20 °C and acclimated before exposure. For treatments, animals were randomly assigned to experimental groups ($n = 3$ per condition; all experiments in triplicate) and anaesthetised in 10% ethanol prior to dissection. Experimental groups were organised as follows:

- Group 1 (control): leeches exposed to HFIP vehicle (0.0035%)
- Groups 2–4: leeches exposed to 0.05, 0.5, and 5 mg L^{-1} PET NPs for 24 hours
- Groups 5–7: leeches exposed to 0.05, 0.5, and 5 mg L^{-1} PET NPs for 48 hours
- Groups 8–10: leeches exposed to 0.05, 0.5, and 5 mg L^{-1} PET NPs for 72 hours

Additional time points of 1 week and 1 month were included for chronic exposure studies.

Histological analysis

For morphological analysis, tissues were fixed in 4% glutaraldehyde (0.1 M cacodylate buffer, pH 7.4) at 4 °C

overnight, washed, and post-fixed in 2% osmium tetroxide for 1 hour in the dark. Samples were dehydrated in graded ethanol (50–100%), cleared in propylene oxide, and embedded in Epon-Araldite 812 epoxy resin (Sigma-Aldrich, Milan, Italy). Sections (0.7 μm) were cut using a Reichert Ultracut S ultramicrotome (Leica, Wein, Austria), stained with crystal violet and basic fuchsin, and observed under a light microscope (Eclipse, Nikon, Tokyo, Japan) and the images were captured with the DS-5M-L1 digital camera (Nikon, Tokyo, Japan). Ultrathin sections (70–80 nm) were obtained with an RMC Power Tome XL (Boeckeler Instruments, USA), placed on copper grids (300 mesh, Sigma-Aldrich, Milan, Italy), counterstained with uranyl acetate and lead citrate, and samples were analyzed with a JEOL1400Plus transmission electron microscope (Centro di Ricerca e Trasferimento Tecnologico – CRIETT, University of Insubria) as described above.

OCT (optimal cutting temperature) embedding and cryosections

Immediately after dissection, tissues were embedded in OCT compound (Tissue-Tek OCT compound, Sakura Finetek, CA, USA), snap-frozen in dry ice and liquid nitrogen, and stored at –80 °C. Cryosections (0.7 μm) were obtained with a Leica CM1850 cryostat, mounted on gelatin-coated slides, and stored at –20 °C until analysis.

Localisation of fluorescent nanoplastics

Cryosections were rehydrated in PBS (138 mM NaCl, 2.7 mM KCl, 4.3 mM Na_2HPO_4 , pH 7.4) and stained with 4,6-diamidino-2-phenylindol (DAPI) (0.1 mg mL^{-1}) for 3–6 minutes. Slides were mounted with Citifluor (Citifluor Ltd., UK) and PET NPs were visualised based on Nile Red fluorescence. Images were observed under a fluorescent microscope, as previously described.

Immunofluorescent assay

Following rehydration, cryosections were blocked in 2% bovine serum albumin (BSA)/0.1% Tween in PBS and incubated with the following primary antibodies: mouse monoclonal α -human cluster of differentiation 31 – CD31 (dilution 1 : 200, Novocastra – Nussloch, Germany), known to react with leech endothelial cells¹⁹ and rabbit polyclonal α -*Hirudo medicinalis* allograft inflammatory factor – *HmAIF1* (dilution 1 : 150, kindly donated by Professor Vizioli – University of Lille, France), recognising leech macrophage-like cells.^{20,21}

After washing, sections were incubated with FITC-conjugated anti-mouse or anti-rabbit secondary antibodies (ThermoFisher Scientific, Waltham, USA, 1 : 300), counterstained with DAPI, and mounted. Negative controls omitted primary antibodies. Samples were observed using appropriate FITC and DAPI filter sets, and images processed using Adobe Photoshop (<https://www.adobe.com/products/photoshop.html>, Adobe System, Inc.).



Acid phosphatase (ACP) histoenzymatic assay

Cryosections, obtained as described above, were rehydrated in PBS for 10 minutes, incubated for 5 minutes in 0.1 M acetic acid–sodium acetate buffer and then, with the reaction mixture (0.1 M sodium acetate–acetic acid buffer, 0.01% naphthol phosphate, 2% *N,N*-dimethylformamide, 0.06% Fast Red, MnCl_2 0.5 nM) for 90 minutes, at 37 °C. After several PBS washings, the slides were mounted with Citifluor (Citifluor Ltd., UK) and observed under the light microscope.

RNA extraction and quantitative PCR (qPCR)

Leech tissues were frozen in liquid nitrogen and crushed with a mortar and pestle. Samples were then resuspended in 1 ml of TRIzol (Life Technologies, Carlsbad, USA), centrifuged at 11 270g for 10 minutes and then incubated for 5 minutes at room temperature. Subsequently, 200 μl of chloroform was added and samples were centrifuged for 15 minutes at 13 700g at 4 °C. Once the different phases were obtained, 500 μl of the supernatant, in which nucleic acids were present, was recovered and gently mixed with 500 μl of isopropanol. After 10 minutes at room temperature, samples were centrifuged for 10 minutes, and the resulting RNA pellets were washed in EtOH 75% and resuspended in DEPC water. Samples were then quantified, and the RNA purity was evaluated with a 1% agarose gel. 2 μg of RNA were retrotranscribed into cDNA using M-MLV reverse transcriptase (Euroclone S.p.a, Pero, Italy) in the presence of oligodT (Invitrogen, Thermo Fisher Scientific, Waltham, USA) of random hexamers in a final volume of 20 μL . Quantitative real-time PCR (qPCR) was carried out in triplicate in a CFX Connect Real Time PCR Detection System (Bio-Rad, Hercules, USA) using the iTaq Universal SYBRTM master mix (BioRad, Hercules, USA) and 0.2 μM each of forward and reverse primer, in a final volume of 15 μL . The primers used for qPCR amplifications were designed with the web-interface software Primer3Plus and are listed in the table below. After initial denaturation, the PCR reaction was performed at 95 °C (10 s), 60 °C (5 s), and 72 °C (10 s) for 39 cycles. Relative gene expressions were calculated using the $\Delta\Delta\text{Ct}$ method, in which the 18S gene was used as housekeeping (Table 1).

Intracellular ROS detection

ROS production was measured using the fluorogenic probe 2',7'-dichlorodihydrofluorescein diacetate (H_2DCFDA) (Molecular Probes, Eugene, OR, USA), which crosses the cell membrane and gets hydrolysed to 2',7'-dichlorofluorescein (DCF). Upon oxidation by ROS, DCF becomes fluorescent. Cryosections of treated and control samples were incubated with 10 μM H_2DCFDA for 30 minutes at 37 °C in the dark and nuclei were counterstained with DAPI. Fluorescence was measured at excitation 488 nm/emission 525 nm using a Nikon fluorescence microscope and digital camera system.

Table 1 Primers used for qPCR analyses

| Target genes | Primers | Product size (bp) |
|-----------------|---|-------------------|
| <i>Hm</i> AIF-1 | Fw: 5'-GACCTCAAAGACAAGCAGGG-3' Rev: 5'-GGCCAATCTTCTCCAGCATC-3' | 229 |
| SOD | Fw: 5'-ATCCTCTTGAACCCACCACA-3' Rev: 5'-ATCTGGACGCACATCTTGT-3' | 95 |
| GST4A | Fw: 5'-AGACACATCGCCAGGACTAA-3' Rev: 5'-ACGGATACACGACTCCAAC-3' | 127 |
| 18S | Fw: 5'-GATGGTGACTCTTGGATAACTTC-3' Rev: 5'-CTGCCTTCTTGGATGTG-3' | 189 |

Statistical analysis

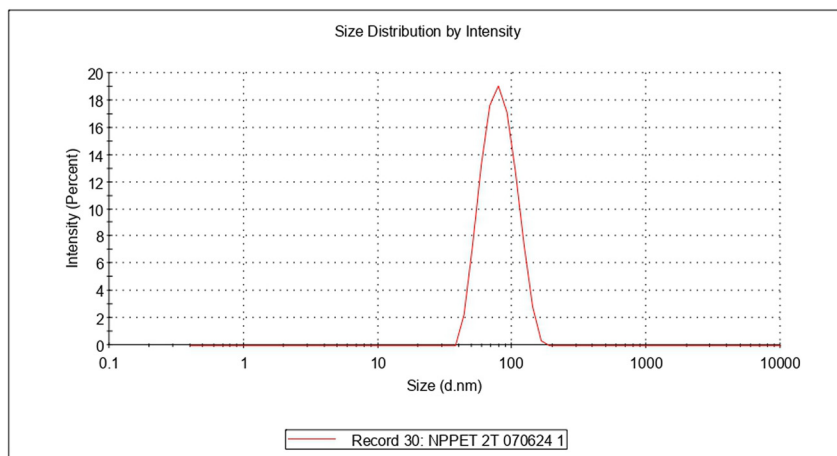
All the experiments were conducted in triplicate and the data show average values \pm standard deviations (SD). The fluorescence analysis for immunolocalisation approaches was performed using the ImageJ software package (<https://imagej.net/ij/index.html>) while the statistical analysis was conducted using the Graph Prism 8 software (GraphPad Software, La Jolla, USA; <https://www.graphpad.com/features>). Both the normality and the homoscedasticity of the samples were assessed using Shapiro–Wilk's and Levene's tests. The significant differences were calculated by one-way ANOVA variance analysis followed by Dunnett's *post hoc* test, in which a *p*-value <0.05 was considered statistically significant and confidence intervals were reported in the SI (S1–S6). In the graphs, the averages with asterisks represent a significant difference between leeches not exposed to or exposed to NPs PP. For immunofluorescence and vascular counts, five random 45 000 μm^2 fields per slide were analysed using ImageJ software.

Results

Characterisation of PET nanoparticles (NPs) and their internalisation in leech tissues

Prior to *in vivo* experiments, PET NPs were characterised using dynamic light scattering (DLS), transmission electron microscopy (TEM) and fluorescence microscopy (Fig. 1A–C). DLS measurements revealed an average diameter of 82.48 ± 24.76 nm, confirming their nanoscale size (Fig. 1A). TEM analysis supported this finding, showing well-defined spherical particles (Fig. 1B). PET NPs were fluorescently labelled using Nile Red, allowing their visualisation under a Cy3 filter (excitation 550–570 nm) (Fig. 1C). The stability of the nanoparticles was further assessed through DLS analyses performed on PET nanoparticles without the fluorescent probe. The results, reported in Fig. S1, showed highly similar size distributions. Freshly prepared nanoparticles displayed a Z-average of 79.08 nm with a polydispersity index (PDI) of 0.071, while samples stored for nine months exhibited a Z-average of 78.69 nm with a PDI of 0.095. The main intensity peaks were centred at approximately 85–86 nm, with comparable standard deviations (24.5 vs. 26.3 nm). These data indicate that the suspensions remained monodisperse and stable over time, with no evidence of significant agglomeration (S7).





Results

Z-Average (d.nm): 75.94

Pdl: 0.083

Intercept: 0.942

Result quality Good

| | Size (d.nm) | % Intensity | St Dev (d.nm) |
|---------|-------------|-------------|---------------|
| Peak 1: | 82.30 | 100.0 | 23.38 |
| Peak 2: | 0.000 | 0.0 | 0.000 |
| Peak 3: | 0.000 | 0.0 | 0.000 |

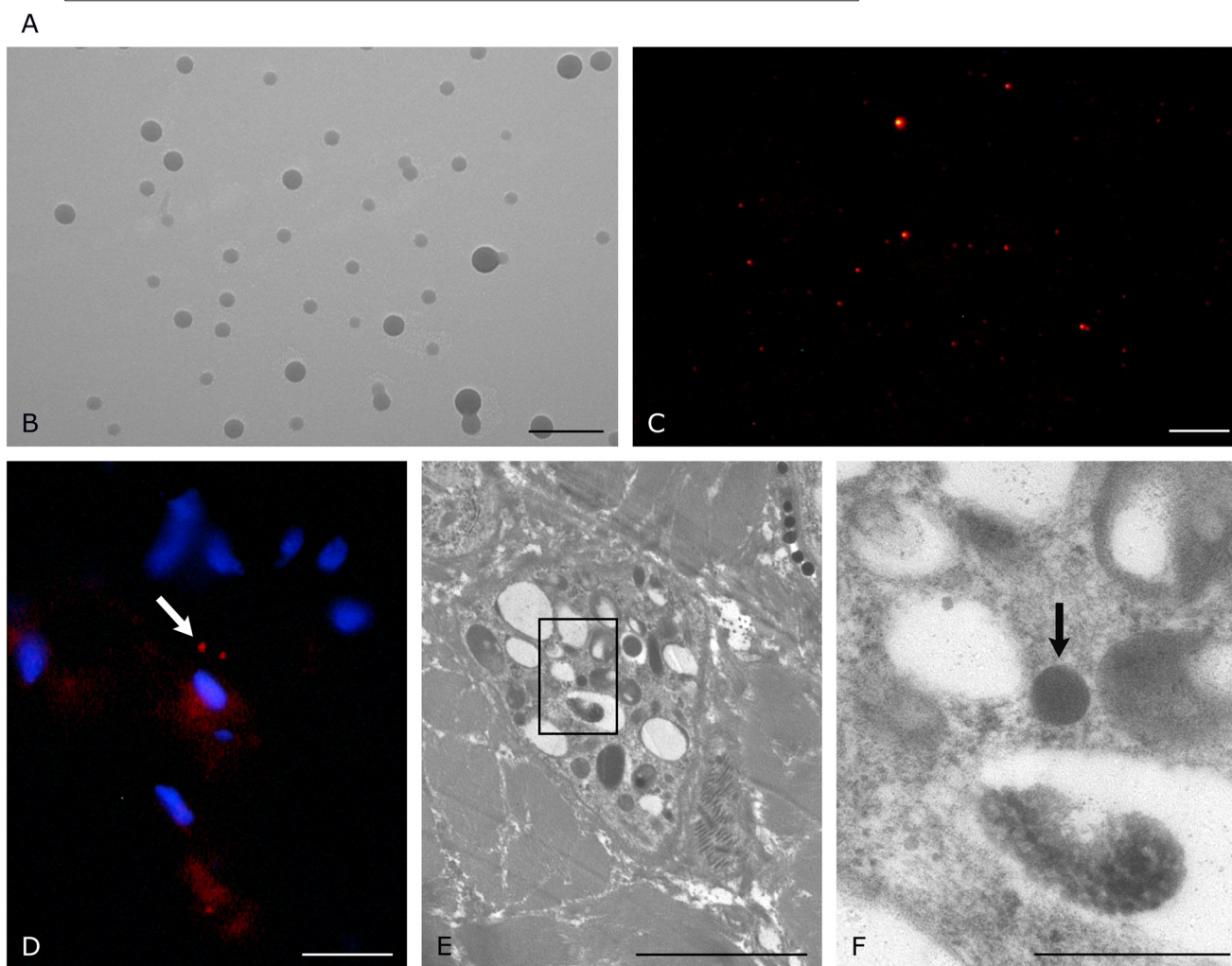


Fig. 1 Characterisation and localisation of PET nanoparticles (NPs) using DLS, TEM, and fluorescence microscopy. (A) Dynamic light scattering (DLS) analysis showing the size distribution of PET NPs by intensity; (B) TEM image illustrating the morphology and size of PET NPs; (C) fluorescence microscopy image of PET NPs; fluorescent PET NPs (white arrows) detected in a cryosection of the leech body wall; cell nuclei are counterstained with DAPI (blue); (E) TEM image showing intracellular localization of PET NPs (arrows); (F) higher-magnification TEM detail of PET NPs highlighted in figure E. Bars in B and E: 2.5 μm ; in C: 100 μm ; in D: 10 μm ; in F: 0.5 μm .

The ability of PET NPs to penetrate *H. verbana* tissues was evaluated using fluorescence and TEM microscopy. Both techniques confirmed the internalisation of PET NPs within

cells, mainly localised in the subepithelial region (Fig. 1D–F), suggesting that active phagocytosis of these exogenous materials may occur.



Morphological response to PET NP exposure

Acute exposure (24–72 hours). Light microscopy analysis revealed that exposure to PET NPs at concentrations of 0.05, 0.5, and 5 mg L⁻¹ for 24, 48, and 72 hours induced a time- and dose-dependent increase in neovascularisation (Fig. 2A–L). In control animals treated with HFIP (hexafluor-2-propanol) solution, the musculocutaneous sac appeared predominantly avascular, with only a few small vessels detectable at all time points (Fig. 2A, E and I). In contrast, leeches exposed to PET NPs showed a progressive and widespread activation of angiogenesis across all exposure times and concentrations. In addition to increased vascularisation, structural remodelling of the botryoidal tissue, a key site involved in vascular development, was evident. In control specimens, this tissue appeared as a compact, cord-like structure composed of tightly connected botryoidal and endothelial cells (Fig. 2M). Following PET NP exposure, even at the lowest concentration, structural alterations were evident: the botryoidal tissue progressively transitioned from a dense, cord-like cellular arrangement to a tubular, pre-vascular structure with lumen formation, even at the lowest concentration tested (Fig. 2N–P).

Quantitative analysis of blood vessels confirmed these morphological observations (Fig. 2Q–S). A significant increase in vessel number was recorded at all time points and across all concentrations compared to controls. Specifically, a clear dose-dependent rise was observed after 24 hours, peaking at 5 mg L⁻¹. After 48 hours, the highest vessel count was recorded at 0.05 mg L⁻¹, while at 72 hours the maximum response occurred at 0.5 mg L⁻¹, suggesting an early and sensitive response to low-dose exposure and highlighting a dynamic and time-dependent modulation of angiogenic activity in response to PET NP exposure.

Chronic exposure (1 week and 1 month). Following the acute exposure experiments, in which PET NPs induced a time- and dose-dependent activation of angiogenesis and remodelling of the botryoidal tissue, additional analyses were performed to assess the effects of chronic exposure. In particular, morphological evaluations were conducted by light microscopy after 1 week and 1 month of continuous exposure to fluorescent PET NPs, to investigate the persistence and progression of angiogenic responses over time (Fig. 3A–H). As expected, in control leeches exposed solely to HFIP, the body wall remained largely avascular (Fig. 3A and E). In contrast, specimens exposed to PET NPs (Fig. 3B–D and F–H) displayed a clear and sustained increase in the number of neo-formed blood vessels at both time points, suggesting that chronic exposure prolongs and reinforces angiogenic activation.

Morphological assessment of botryoidal tissue (Fig. 3I–L) revealed that while in control animals (Fig. 3I) it appeared as a compact cord-like structure with closely packed endothelial and botryoidal cells, chronic exposure to PET NPs induced a progressive transition toward prevascular tubular structures (Fig. 3J–L).

To further validate these findings, vessel counts were performed and the results plotted in corresponding graphs

(Fig. 3M and N). After 1 week, a statistically significant, dose-dependent increase in blood vessel number was observed across all tested concentrations. Similarly, after 1 month, vascularisation remained elevated, with the most pronounced effect recorded at 0.5 mg L⁻¹, indicating a persistent pro-angiogenic response following long-term nanoplastic exposure.

Endothelial activation: CD31 expression

Acute exposure (24–72 hours). To validate the morphological findings, immunofluorescence analyses were performed on both untreated and PET NP-treated leeches using an anti-CD31 antibody, a specific marker for endothelial cells (Fig. 4). In control animals, the CD31 signal was consistently low at all time points (Fig. 4A, E and I), with only a few CD31⁺ cells observed beneath the epithelium and around inner muscle fibres, confirming the predominantly avascular state seen in morphological sections. In contrast, leeches exposed to PET NPs exhibited a marked increase in CD31 immunoreactivity across all concentrations and time points (Fig. 4B–D, F–H and J–L). After 24 hours, fluorescence intensity was higher in all treated groups (Fig. 4B–D) compared to the control (Fig. 4A). At 48 hours, the strongest signal was detected at the lowest concentration (0.05 mg L⁻¹), although increased CD31⁺ cell presence was observed at all tested doses (Fig. 4F–H). By 72 hours, a concentration-dependent increase in CD31 expression was evident, with the highest intensity recorded at 5 mg L⁻¹ (Fig. 4J–L).

No signal was detected in negative controls lacking the primary antibody (S8). Quantification of CD31 fluorescence intensity confirmed these observations, showing a significant increase in endothelial marker expression in all PET NP-treated samples (Fig. 4N–P).

Chronic exposure (1 week and 1 month). Following the confirmation of angiogenic activation in acute exposure through CD31 immunofluorescence, additional analyses were conducted to assess whether this response persisted after chronic exposure to PET NPs. Immunofluorescence staining using anti-CD31 antibody was performed on leeches exposed to PET NPs for 1 week and 1 month, in order to detect the presence and distribution of endothelial cells and new blood vessels, as previously observed in morphological sections.

In control animals not exposed to plastics, the CD31 signal remained low, with only a few positive cells located beneath the epithelium and around muscle fibres (Fig. 5A and E). In contrast, leeches treated with PET NPs showed a significant and dose-dependent increase in CD31 immunoreactivity at both time points (Fig. 5B–D and F–H), confirming the persistence of endothelial activation during chronic exposure.

Negative control sections in which the primary antibody was omitted showed no detectable signal (S8), validating the specificity of the staining.

To further support these findings, CD31 fluorescence intensity was quantified (Fig. 5I and J). After 1 week, all tested concentrations induced a statistically significant increase in



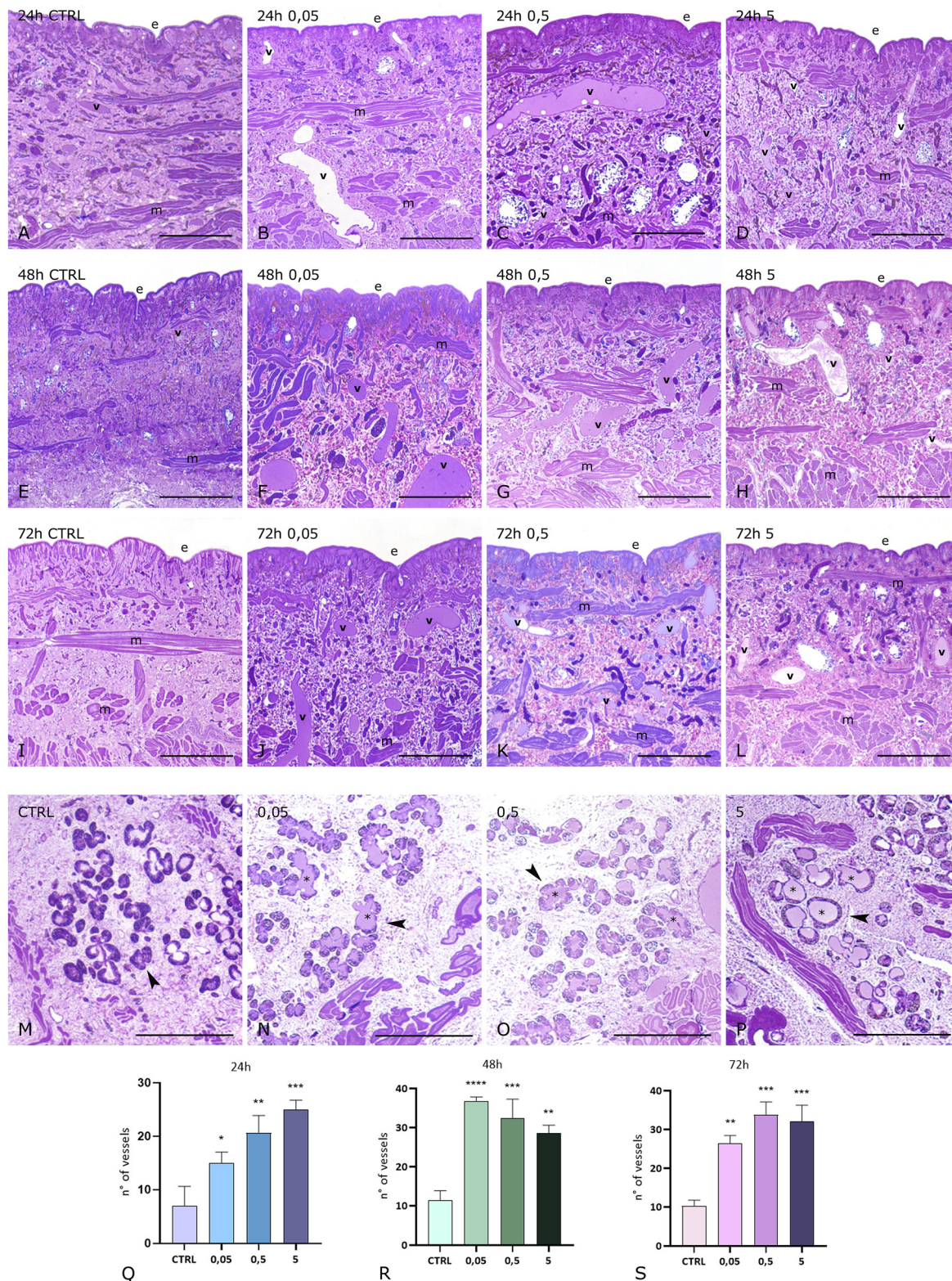


Fig. 2 PET NPs induce angiogenesis and structural remodelling of botryoidal tissue in *H. verbanda*. Light microscopy images of the leech body wall following exposure to PET NPs at 0.05, 0.5, and 5 mg L⁻¹ for 24, 48, and 72 hours (A–L). Control tissues (A, E and I) appear largely avascular. Treated samples exhibit increased neovascularisation throughout the musculocutaneous sac (B–D, F–H, J–L). In controls (M), botryoidal tissue (arrowheads) appears as a compact cord-like structure. In PET NP exposed leeches (N–P) pre-vascular phenotype with lumen (asterisks) formation is visible. Graphs (Q–S) show vessel quantification, confirming a significant increase in vessel number at all time points and concentrations compared to controls. A dose-dependent increase is observed after 24 hours, with a peak at 5 mg L⁻¹; at 48 hours, the highest vessel count occurs at 0.05 mg L⁻¹; and at 72 hours, the peak response is observed at 0.5 mg L⁻¹. In the graphs, * means that $p < 0.05$; ** means that $p < 0.01$; *** means that $p < 0.001$. e epithelium, m muscle, v vessels. Bars in A–P: 100 μ m.



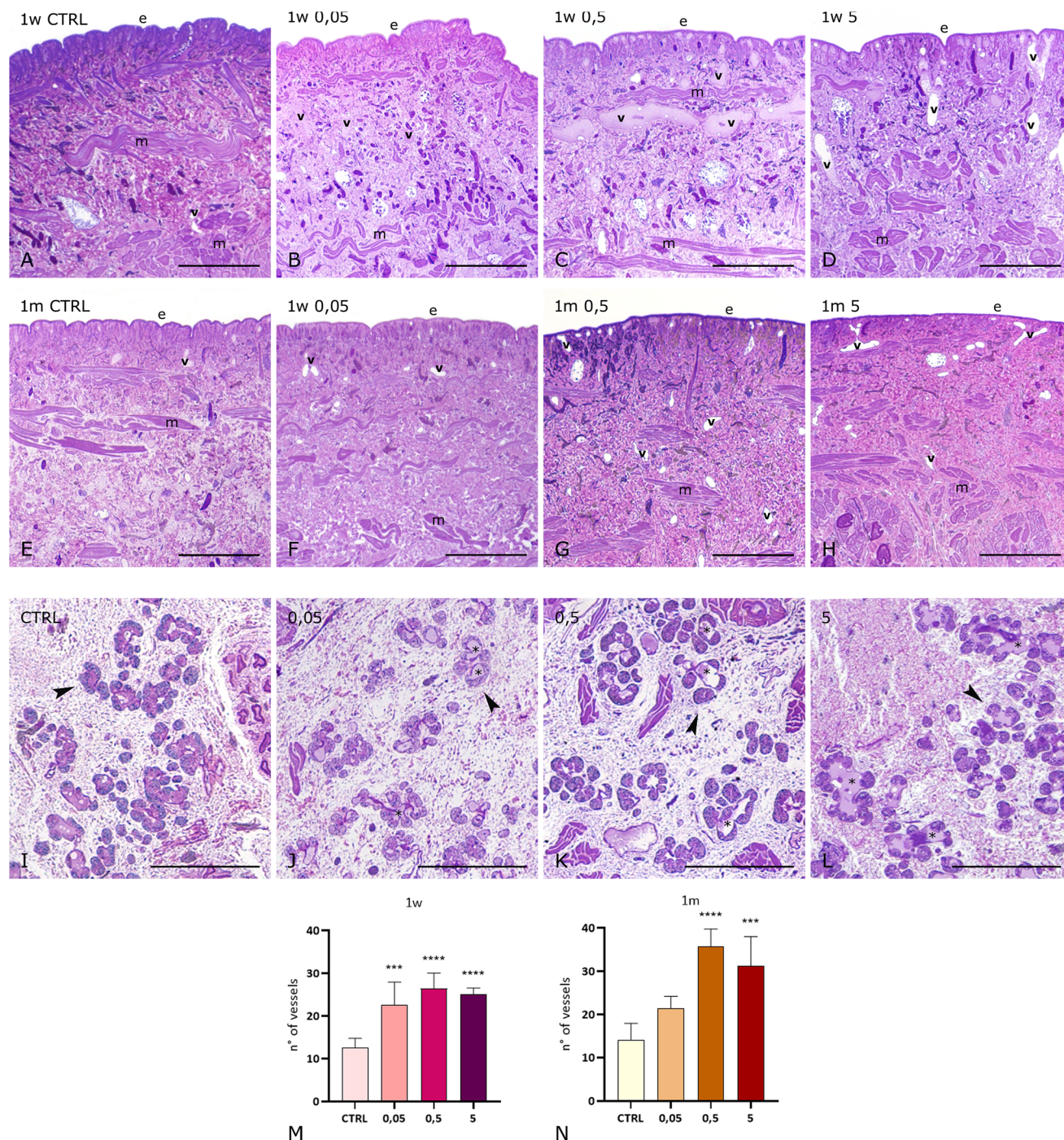


Fig. 3 Chronic exposure to PET NPs induces persistent angiogenesis and remodelling of botryoidal tissue in *H. verbana*. Light microscopy images of the leech body wall after 1 week (A–D) and 1 month (E–H) of exposure to PET NPs at 0.05, 0.5, and 5 mg L⁻¹. Control animals (A and E) display avascular tissues, while treated leeches show increased neovascularisation in a dose-dependent manner (B–D and F–H). In control leeches (I), botryoidal tissue (arrowheads) has a cord-like shape. Upon PET NP exposure (J–L), prevascular structures with open lumens (asterisks) are evident. Graphs (M and N) show quantitative vessel counts, confirming a statistically significant, dose-dependent increase in vascularisation after 1 week at all concentrations, and a persistent angiogenic effect after 1 month, with the highest significance at 0.5 mg L⁻¹. In the graphs, *** means that $p < 0.001$; **** indicates $p < 0.0001$. e epithelium, m muscle, v vessels. Bars in A–L: 100 μ m.

CD31 expression. At 1 month, the signal remained elevated, with significant effects observed at the intermediate (0.5 mg L⁻¹) and highest (5 mg L⁻¹) concentrations, suggesting a sustained pro-angiogenic effect over time.

Macrophage-like cell activation: ACP histoenzymatic assays

Acute exposure. In the medicinal leech, macrophage-like cells play a fundamental role in the innate immune response by



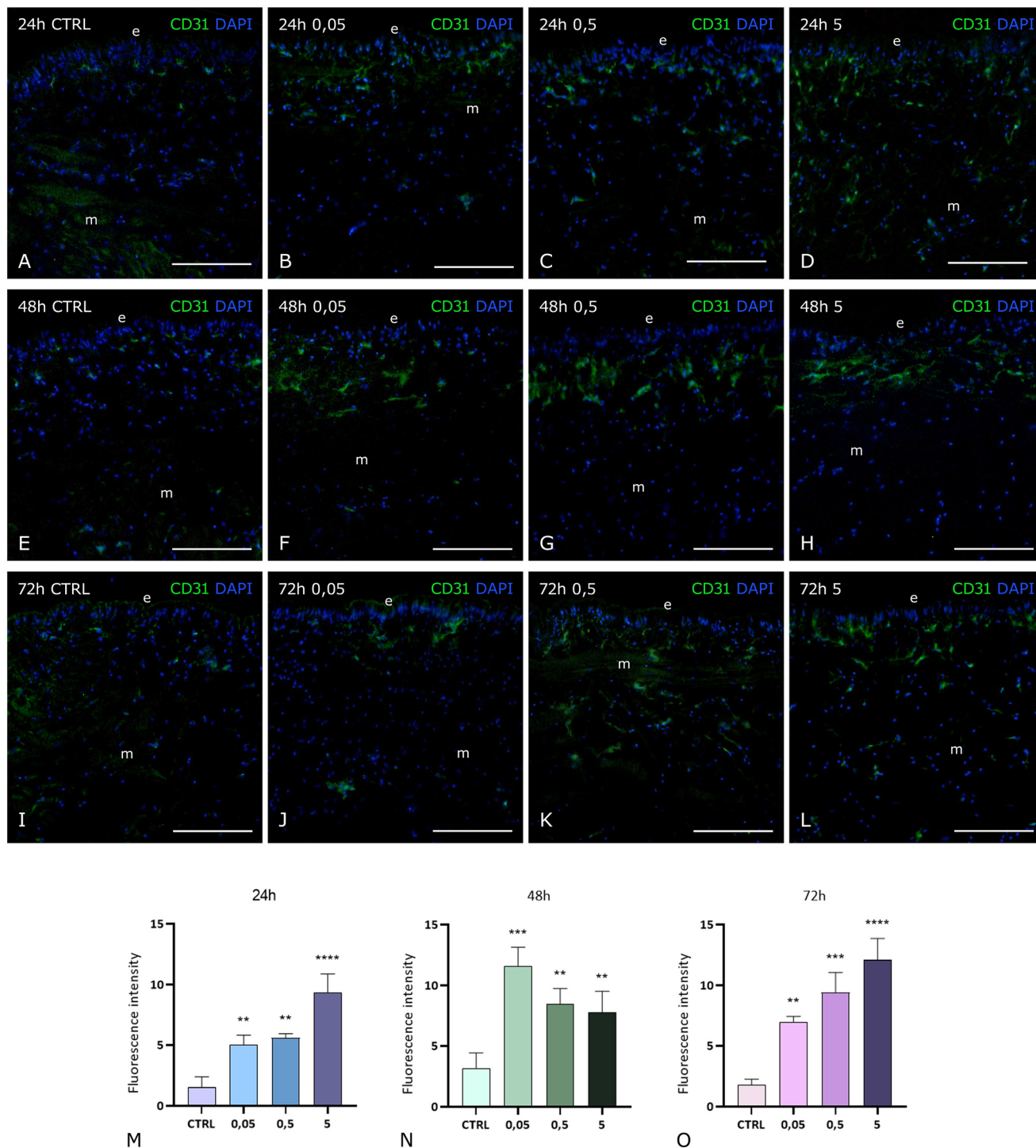


Fig. 4 PET NPs induce CD31 expression in *H. verbanda*, confirming angiogenic activation. Immunofluorescence staining with anti-CD31 antibody in the leech body wall after exposure to PET NPs at 0.05, 0.5, and 5 mg L⁻¹ for 24, 48, and 72 hours (A–L). In untreated controls (A, E and I), only a weak CD31 (in green) signal is detected, indicating limited endothelial presence. PET NP-treated leeches show increased CD31 immunoreactivity at all concentrations and time points (B–D, F–H and J–L). At 24 hours, the signal intensity is elevated in all treated groups. At 48 hours, the strongest response is observed at 0.05 mg L⁻¹, while at 72 hours the fluorescence intensity increased with dose, peaking at 5 mg L⁻¹. Graphs (M–O) show quantification of CD31 fluorescence intensity, confirming a significant increase in endothelial marker expression in all PET NP-exposed groups compared to controls. In the graphs, *** means that $p < 0.001$; **** indicates $p < 0.0001$. e epithelium, m muscle, in blue are nuclei stained with DAPI. Bars in A–L: 100 μ m.

recognising and eliminating non-self elements, such as pathogens and xenobiotics, through phagocytosis and encapsulation. To confirm the recruitment and activation of these innate immune

cells, previously suggested by TEM analysis, a histochemical acid phosphatase (ACP) assay was performed on leech tissues exposed to all concentrations and time points (Fig. 6).



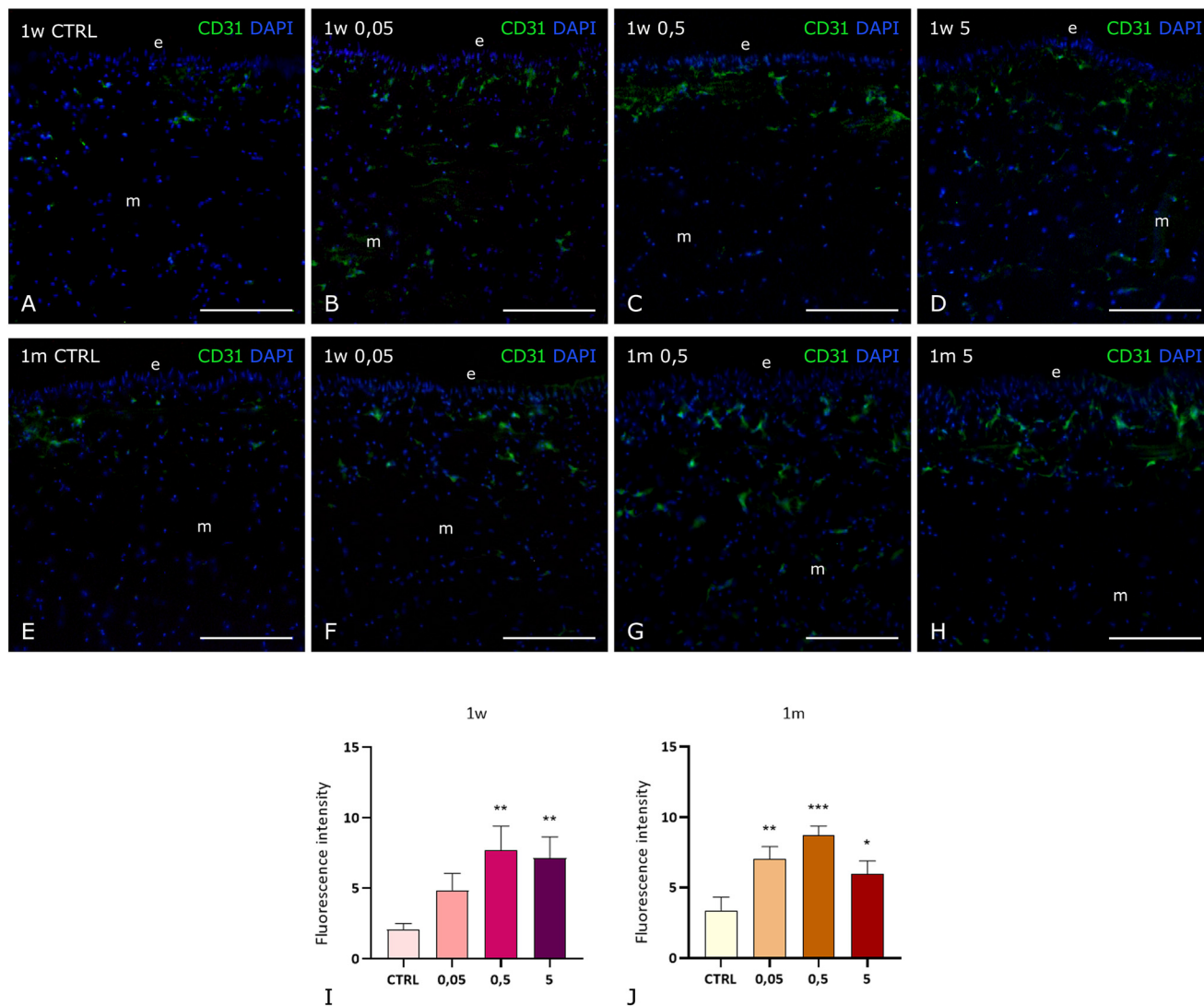


Fig. 5 Chronic exposure to PET NPs sustains CD31 expression and endothelial activation in *H. verbana*. Immunofluorescence images of the leech body wall stained with anti-CD31 antibody after 1 week (A–D) and 1 month (E–H) of exposure to PET NPs at 0.05, 0.5, and 5 mg L⁻¹. In untreated controls (A and E), a weak CD31 signal is detected, indicating minimal vascular presence. Treated animals show a clear, dose-dependent increase in CD31⁺ endothelial cells at both time points (B–D and F–H). Graphs (I and J) show quantification of CD31 fluorescence intensity, confirming a statistically significant increase after 1 week at all concentrations and after 1 month at 0.5 and 5 mg L⁻¹. In the graphs, * means that $p < 0.05$; ** means that $p < 0.01$; *** means that $p < 0.001$. e epithelium, m muscle, in blue are nuclei stained with DAPI. Bars in A–H: 100 μ m.

In control specimens not exposed to PET NPs (Fig. 6A, E and I), only a few ACP⁺ cells were detectable, as expected under normal physiological conditions. Following PET NP exposure, a dose-dependent increase in ACP⁺ cells was observed at all three time points (Fig. 6B–D, F–H and J–L). While tissues exposed to the lowest concentration showed results similar to controls (Fig. 6B and F), a marked accumulation of ACP⁺ cells was visible at 0.5 and 5 mg L⁻¹, localised within the musculocutaneous sac and underneath the epithelial surface (Fig. 6C, D, G, H, K and L).

Quantitative analysis of ACP⁺ cells confirmed these histochemical results, showing a trend consistent with the microscopic observations (Fig. 6M–O).

Chronic exposure. To further investigate the long-term immune response to PET nanoplastics, the ACP

histoenzymatic assay was performed after 1 week and 1 month of exposure (Fig. 7A–H). As observed in the acute phase, the number of ACP⁺ cells increases after exposure to PET NPs. After 1 week, the number of phagocytically active cells increased in a dose-dependent manner, with most ACP⁺ cells located beneath the epithelium (Fig. 7B–D). At 1 month, numerous ACP⁺ cells were still detectable, particularly in leeches treated with 0.5 mg L⁻¹, and appeared to migrate from the inner body wall toward the epithelium (Fig. 7F–H), suggesting a sustained and spatially organised immune reaction. The quantification of ACP⁺ cells (Fig. 7I and J) confirmed the histological observations, showing a statistically significant increase at all concentrations after 1 week, and a persistent elevation, most marked at 0.5 mg L⁻¹, after 1 month of exposure.



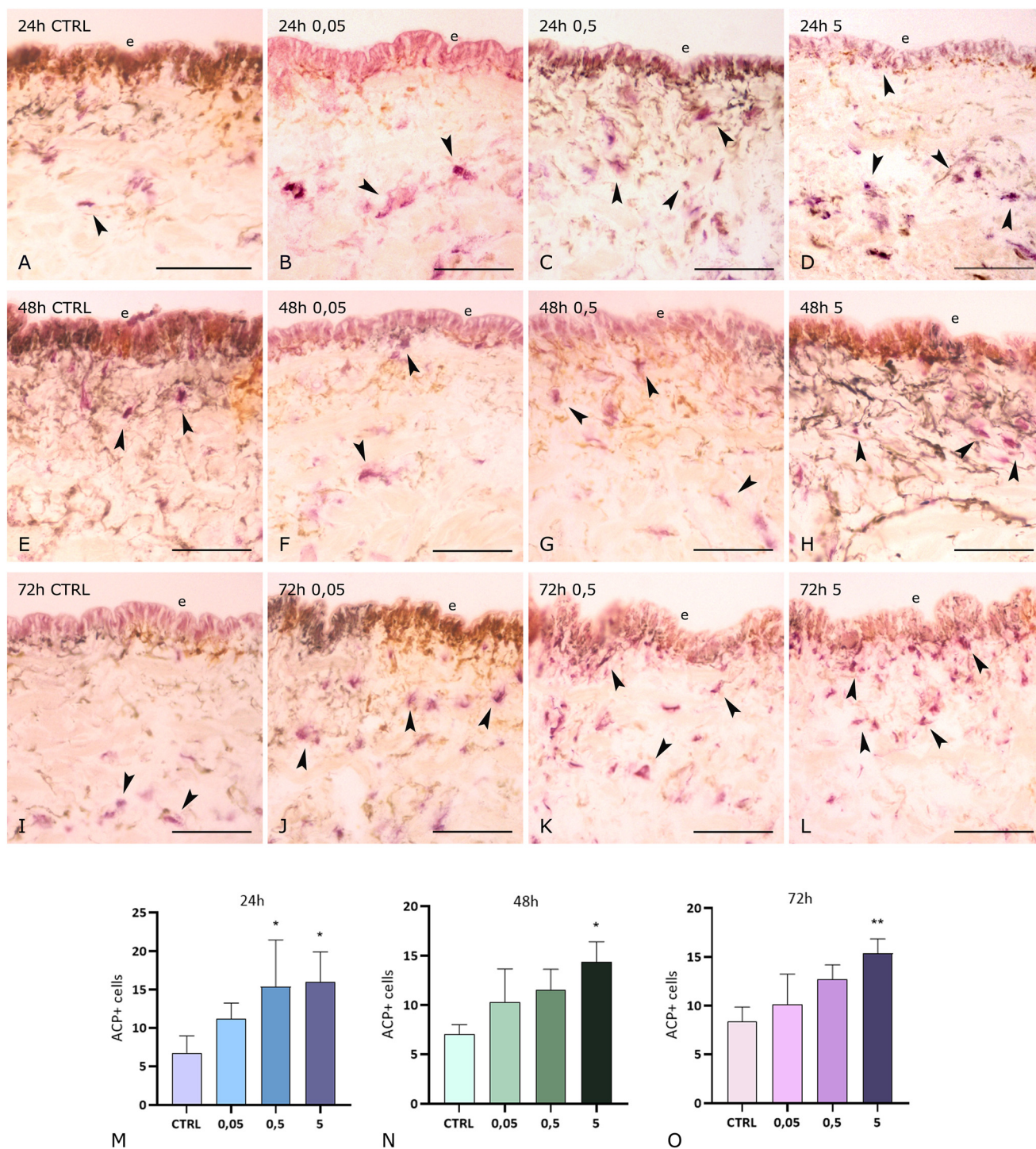


Fig. 6 PET NPs modulate the recruitment of ACP⁺ cells in *H. verana*. ACP histoenzymatic staining of leech body wall sections following exposure to PET NPs at 0.05, 0.5, and 5 mg L⁻¹ for 24, 48, and 72 hours. In control samples (A, E and I), only a few ACP⁺ cells are visible. In treated samples (B–D, F–H and J–L), a dose-dependent increase in ACP⁺ cell number is observed, with the most evident activation at intermediate and high concentrations. Graphs (M–O) show the quantification of ACP⁺ cells, confirming the temporal and concentration-dependent dynamics of macrophage activation. In the graphs, * means that $p < 0.05$; ** means that $p < 0.01$. e epithelium, arrowheads ACP⁺ cells. Bars in A–L: 100 μ m.

*Hm*AIF-1 as a marker of inflammation and macrophage-like cells

Acute exposure and chronic exposure. To further investigate the activation and recruitment of macrophage-like

cells in response to PET NPs, the expression of *Hm*AIF-1, a macrophage-specific pro-inflammatory cytokine, was analysed through qPCR and immunofluorescence (Fig. 8). After acute exposure, qPCR analysis revealed an increase in *Hm*AIF-1



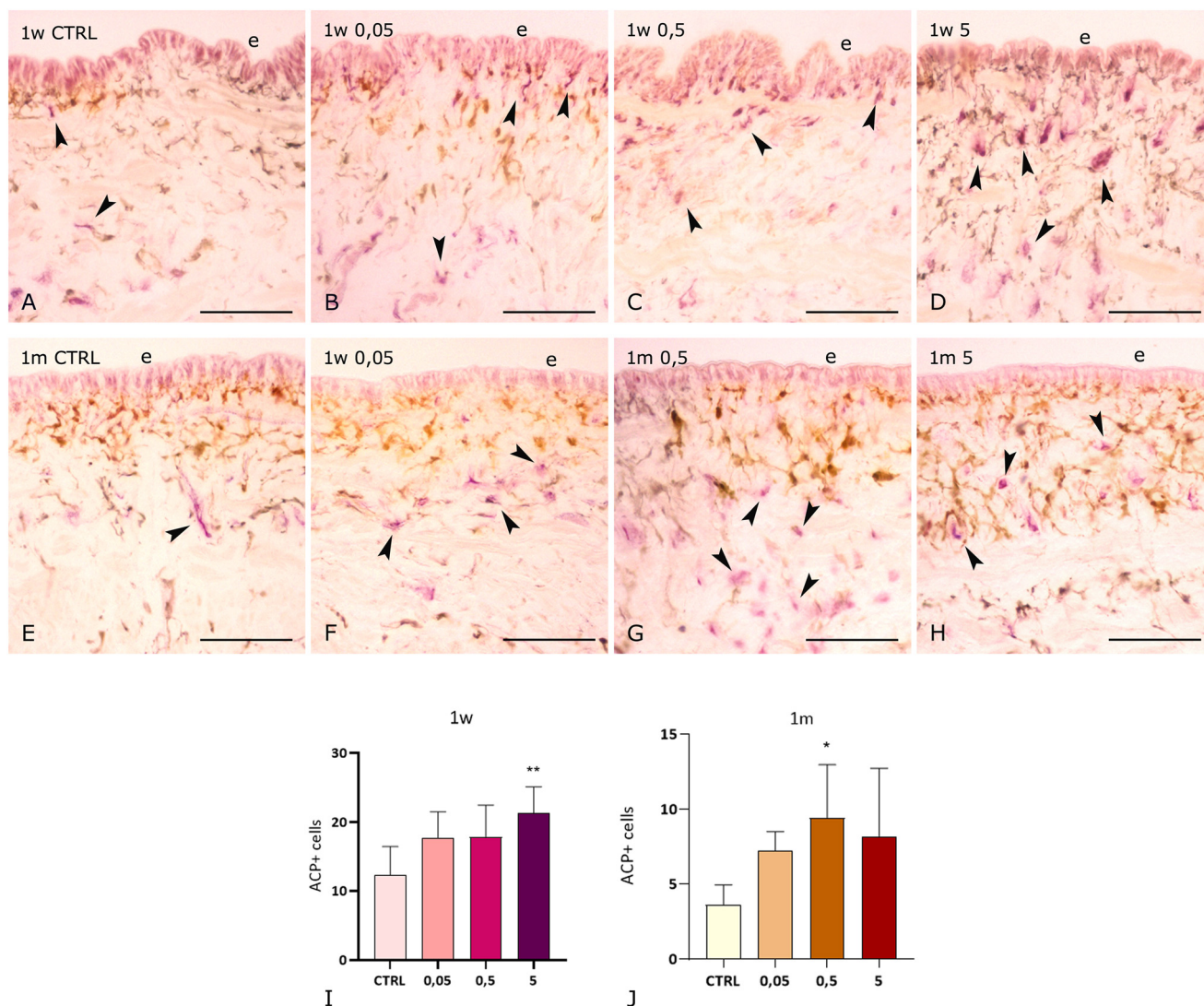


Fig. 7 Chronic exposure to PET NPs activates ACP⁺ cells in the *H. verbana* body wall. ACP histoenzymatic staining reveals the presence of phagocytically active ACP⁺ cells after 1 week (A–D) and 1 month (E–H) of exposure to PET nanoplastics at concentrations of 0.05, 0.5, and 5 mg L⁻¹. In control samples (A and E), few ACP⁺ cells are observed. Treated specimens show a dose-dependent increase in ACP⁺ cells after 1 week (B–D), with strong localisation near the epithelium. After 1 month (F–H), numerous activated ACP⁺ are visible, particularly at 0.5 mg L⁻¹, migrating toward the outer tissue layers. Graphs (I and J) quantify the total number of ACP⁺ cells after 1 week (I) and 1 month (J) from treatment, confirming the microscopic results. In the graphs, * means that $p < 0.05$; ** means that $p < 0.01$. e epithelium, arrowheads ACP⁺ cells. Bars in A–L: 100 μ m.

mRNA expression at all time points (Fig. 8A, D and G). While no upregulation in gene expression was evident at the lower NP concentration, a significant increase in gene expression was detected at 0.5 and 5 mg L⁻¹, confirming a dynamic modulation of the inflammatory response in correlation with nanoparticle concentration and exposure time. Based on these results, immunofluorescence analyses were conducted comparing control tissues with those treated at the highest concentrations. In control leeches, only a few *HmAIF-1*⁺ cells were detected beneath the epithelium (Fig. 8B, E and H). In contrast, PET NP-exposed tissues displayed a significant increase in *HmAIF-1* signal, particularly at the higher concentration (Fig. 8C, F and I), supporting the involvement of activated macrophage-like cells during the inflammatory response.

For the chronic exposure, immunolocalisation was performed at 1 week and 1 month (5 mg L⁻¹), based on previous ACP data. In untreated animals (Fig. 8K and N), a low signal was again observed, while in treated animals after 1 week, the number of *HmAIF-1*⁺ cells clearly increases in the subepithelial region, indicating a persistent immune cell activation. However, after 1 month of exposure to the highest PET NP concentration, a reduced number of positive cells, comparable to that observed in control samples, was detected. qPCR results at 1 week and 1 month (Fig. 8J and M) further confirmed these findings. After 1 week, a dose-dependent increase in *HmAIF-1* gene expression was detected, with peak expression at 5 mg L⁻¹. After 1 month, a nonlinear trend was observed: a slight increase at 0.05 mg L⁻¹, a marked and statistically significant peak at 0.5 mg L⁻¹, followed by a decrease at 5 mg L⁻¹. These data supported the



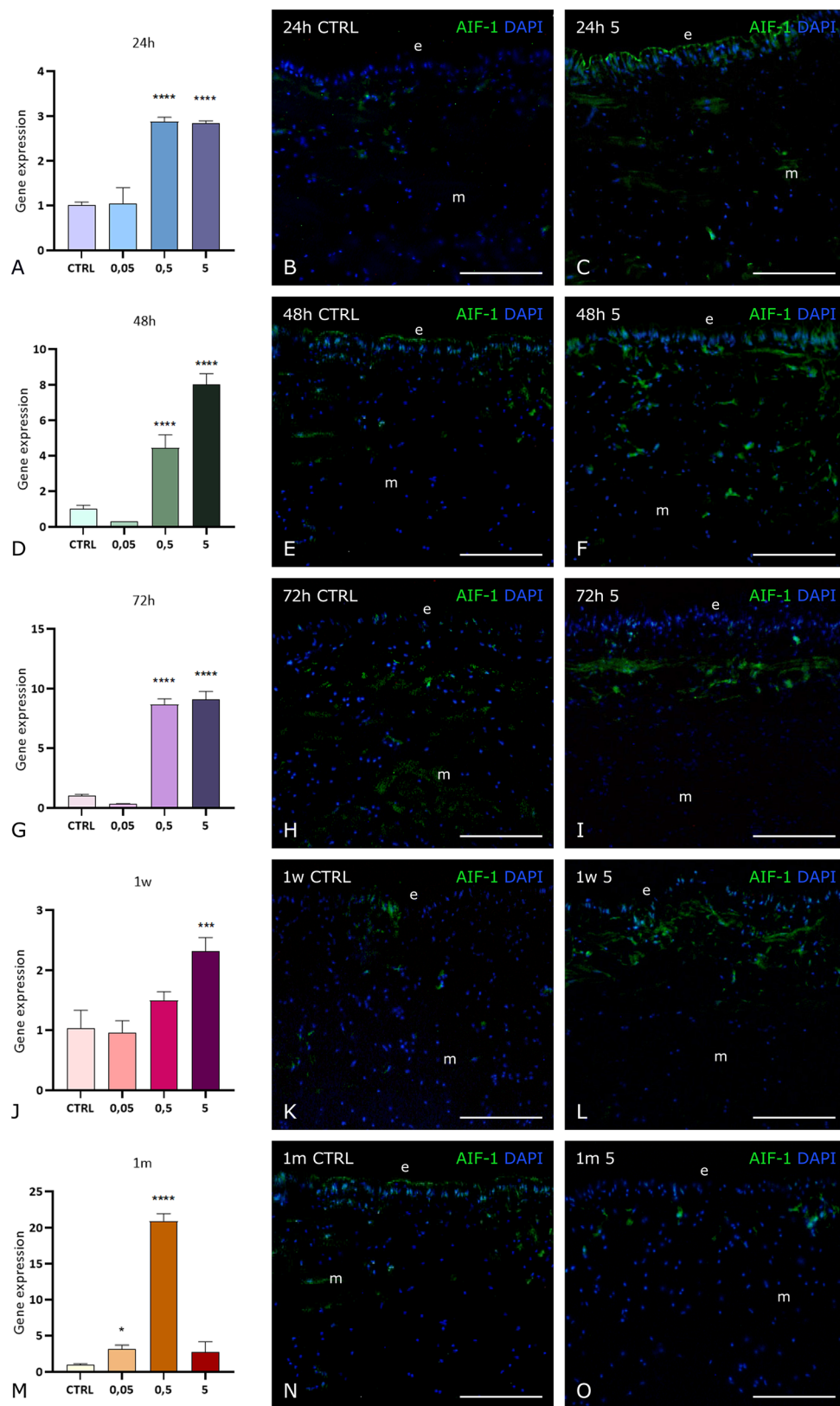


Fig. 8 *HmAIF-1* expression reveals macrophage-like cell activation following acute and chronic PET NP exposure. Immunofluorescence images showing *HmAIF-1* expression in control (B, E and H) and PET NP-treated leeches at the highest concentration after acute exposure (C, F and I). Relative *HmAIF-1* mRNA levels (qPCR) at 24, 48, and 72 hours (A, D and G), showing dose-dependent expression patterns. *HmAIF-1* immunolocalisation under chronic exposure: control samples (K and N) and samples exposed to 5 mg L⁻¹ for 1 week and 1 month (L and O). qPCR quantification of *HmAIF-1* gene expression after 1 week and 1 month (J and M), confirming increased expression in treated samples. In the graphs, * means that $p < 0.05$; *** means that $p < 0.001$; **** indicates $p < 0.0001$. e epithelium, m muscle. Bars in B, C, E, F, H, I, K, L, N and O: 100 μ m.



immunofluorescence and morphological observations, reinforcing the key role of *Hm*AIF-1 in mediating macrophage-like cell activation during the inflammatory response to PET nanoplastics.

Assessment of oxidative stress induced by PET NPs

Acute exposure and chronic exposure. Plastic nanoparticles are well known to induce oxidative stress, primarily through the generation of reactive oxygen species (ROS) that disrupt cellular redox homeostasis. To investigate the antioxidant response elicited by PET NPs in *H. verbana*, qPCR analyses were performed to quantify the expression levels of two key antioxidant enzymes: glutathione *S*-transferase (*GST4A*) and superoxide dismutase (*SOD*) (Fig. 9). In the acute exposure, both *GST4A* and *SOD* genes showed a dose-dependent increase in expression at all tested time points (24, 48, and 72 hours), with maximum expression levels observed at the highest concentration (5 mg L⁻¹) (Fig. 9A–F). These findings indicated that PET NPs rapidly triggered an oxidative stress response, leading to upregulation of protective antioxidant mechanisms.

In chronic exposure, gene expression patterns appeared less linear and more dynamic. Regarding *SOD*, a moderate increase in mRNA expression was noted after 1 week, especially at higher concentrations (Fig. 9G). After 1 month, however, *SOD* expression significantly increased only at 0.5 mg L⁻¹, remaining notably low at the lowest and highest concentrations (Fig. 9I). For *GST4A*, after 1 week of exposure, gene expression initially decreased at the lowest concentrations, followed by a significant upregulation at 5 mg L⁻¹ (Fig. 9H). However, at 1 month, peak expression was recorded at 0.5 mg L⁻¹, with a marked decline at 5 mg L⁻¹ (Fig. 9J), suggesting a time-dependent modulation of *GST4A* activity, possibly due to cellular adaptation or damage. This result was consistent with the *SOD* pattern and further supported the idea that the intermediate concentration may trigger a more effective or sustained antioxidant response, whereas extreme concentrations may lead to cellular exhaustion or toxicity. Comparable results were obtained by evaluating ROS (reactive oxygen species) production through the 2',7'-dichlorodihydrofluorescein diacetate (H₂DCFDA) assay, as shown in SI (S9).

These findings clearly demonstrated that PET NP exposure induces oxidative stress, as evidenced by the transcriptional activation of *GST* and *SOD*, and that this response is both time- and dose-dependent. Furthermore, the production of ROS was significantly modulated following exposure, confirming that PET NPs trigger an imbalance between ROS generation and cellular antioxidant defences. This imbalance leads to oxidative damage and contributes to the observed cellular stress response, consistent with previous reports on nanoparticle-induced oxidative mechanisms.

Discussion

The widespread environmental distribution of nanoplastics (NPs) and their accumulation in freshwater ecosystems pose a growing threat to aquatic organisms. Among these

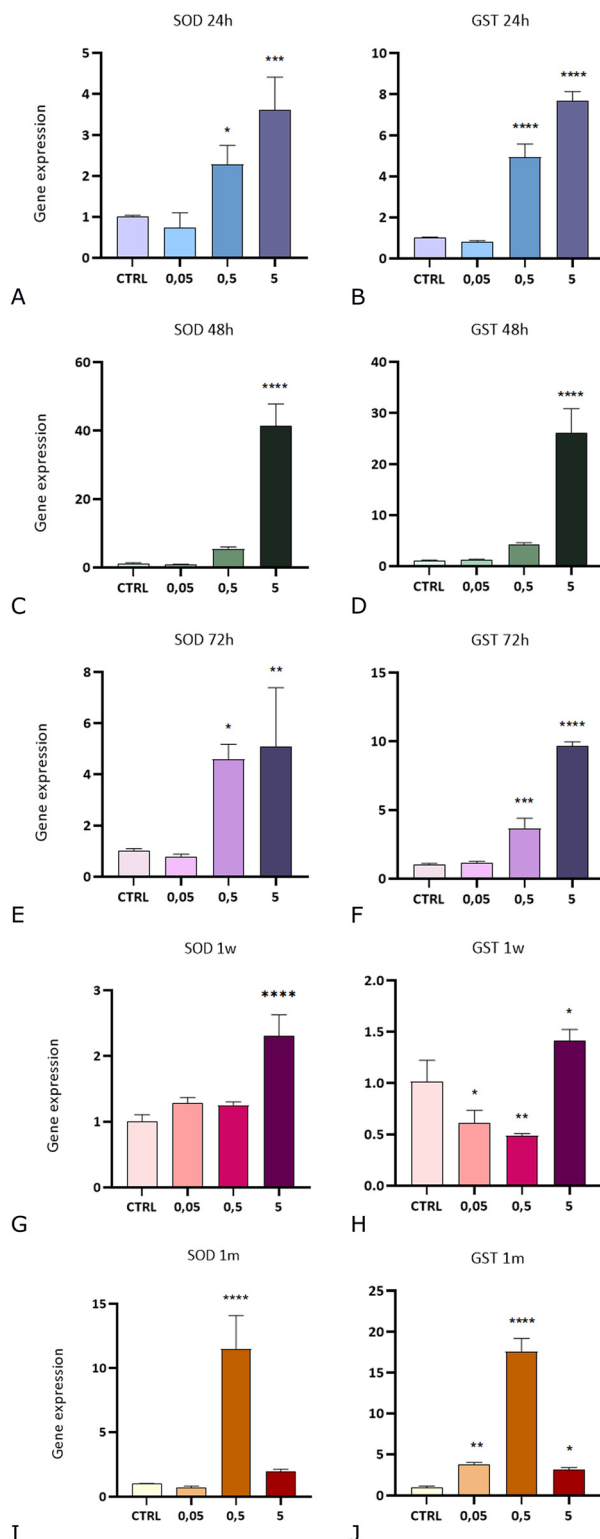


Fig. 9 Expression of antioxidant enzymes *SOD* and *GST4A* in response to PET NP exposure. Relative mRNA levels of *SOD* and *GST4A* after 24, 48, and 72 hours of PET NP exposure (A–F), showing a dose-dependent upregulation, with peak expression at 5 mg L⁻¹. Gene expression of *SOD* and *GST4A* after 1 week and 1 month of chronic exposure (G–J). A significant increase at 0.5 mg L⁻¹ was observed for both enzymes at 1 month, while expression at 5 mg L⁻¹ declined. In the graphs, * means that $p < 0.05$; ** means that $p < 0.01$; *** means that $p < 0.001$; **** indicates $p < 0.0001$.



contaminants, PET nanoplastics, derived from the degradation of widely used consumer products, are of particular concern due to their environmental persistence, nanoscale dimensions, and high surface reactivity.

In this study, we examined the biological effects of both acute and chronic PET NP exposure in *H. verbana*, a freshwater annelid increasingly recognised as a valuable model in ecotoxicology owing to its accessible immune and vascular systems and evolutionary conservation of stress-response pathways. By integrating histological, molecular, and immunological approaches, we demonstrate that *H. verbana* elicits a multifactorial and time-dependent response to PET NP exposure, including activation of immune defences, oxidative stress responses, angiogenesis, and tissue remodelling. These results are consistent with previous findings on the effects of polypropylene (PP) micro- and nanoplastics in the same model¹² and parallel responses observed in other aquatic invertebrates^{22–24} and vertebrate models.^{25,26}

PET nanoplastics were readily internalised by leech tissues, as confirmed by fluorescence and electron microscopy, which detected particles beneath the epithelium and within macrophage-like cells. These data suggest that the mucosal epithelium of *H. verbana* provides limited protection against nanoparticle penetration, likely due to the small size and high diffusibility of PET NPs. The observed phagocytic uptake and recruitment of ACP⁺ immune cells indicate a rapid recognition of PET NPs as non-self, triggering innate immune responses similar to those reported in molluscs, crustaceans, and teleosts.^{27,28} Both acute and chronic exposures induced significant upregulation of the macrophage marker *HmAIF-1*, with acute exposure yielding a dose-dependent increase, while chronic exposure, particularly at 1 month, revealed a biphasic response: maximal expression at intermediate concentrations and reduction at the highest dose. Rather than a simple decrease, this pattern likely reflects a complex immune regulation where moderate doses stimulate macrophage activation, but excessive exposure leads to immune exhaustion or engages negative feedback mechanisms intended to prevent tissue damage caused by chronic inflammation. Such downregulation at high exposure levels has parallels in other invertebrate species, suggesting a conserved adaptive response that balances immune activation with avoidance of detrimental hyperinflammation.^{29–31} ACP and *HmAIF-1* were selected due to their well-established roles as markers of innate immune activation and macrophage responses in *H. verbana*. Classical inflammatory cytokines such as TNF- α and IL-1 β , widely studied in vertebrates, have less characterised homologs and functional roles in annelids, and current molecular tools for their detection are limited or unavailable in this species. Therefore, ACP and *HmAIF-1* remain the most reliable markers to monitor inflammatory activation in this model organism under environmental stress.

Similar dynamics were previously reported in *H. verbana* exposed to per- and polyfluoroalkyl substances (PFAS), where high concentrations resulted in immunosuppression and downregulation of inflammatory genes.¹³ Analogous biphasic or

hormetic responses have also been documented in *M. galloprovincialis* and *E. foetida* exposed to nanoplastics, metals, or pesticides, indicating that immune tolerance or physiological compensation may occur in invertebrates under chronic or high-dose stress.^{30,31} The uptake of PET nanoplastics in *H. verbana* is likely mediated primarily *via* the gut and mucosal epithelial surfaces, which serve as the first barrier against environmental contaminants. Epithelial cells, with their dynamic turnover and barrier functions, play a critical role in limiting nanoparticle penetration while also orchestrating immune and oxidative stress responses upon exposure. In particular, mucus secretion from specialised epithelial cells creates both a physical and chemical barrier that may trap and neutralise nanoparticles, reducing their direct contact with underlying tissues and modulating inflammation. The mucus is rich in glycoproteins and antioxidant molecules, contributing to chemical detoxification and protection against oxidative damage. These features suggest that the interplay between gut epithelium and mucus secretion constitutes a key frontline defence mechanism in the organism's response to nanoplastic contamination. This involvement of mucus cells has been previously observed in the leeches *H. verbana*¹² and *Erpobdella johanssoni*,²² specifically in response to microplastic exposure. Further exploration of this interaction could provide valuable insights into the early stages of nanoparticle uptake and the cascade of downstream biological effects observed in this and similar aquatic invertebrates. Vascular and hematopoietic tissues also exhibited marked changes, particularly in the botryoidal tissue, a key hematopoietic structure in leeches. Light microscopy and immunofluorescence analyses revealed neovascularisation and a transition from a cord-like to tubular morphology, suggestive of vasculogenic remodelling. These alterations were associated with increased expression of CD31, a conserved endothelial marker, and were most prominent after high-dose acute exposure. Such responses likely reflect compensatory mechanisms to mitigate inflammation- or hypoxia-induced tissue damage and are in line with responses observed in other aquatic species under toxic stress.^{33,34} Notably, beyond its structural plasticity, the botryoidal tissue plays a central role in immune cell production and release. Angiogenesis in this context may facilitate the recruitment and trafficking of circulating immune effectors, ensuring a rapid and localised response to PET NP-induced injury. The remodelling of this hematopoietic-vascular niche under toxic stress may thus represent a key mechanism linking inflammation with tissue repair and immune surveillance in leeches.^{14,22}

A noteworthy aspect of the vascular response observed in the acute exposure groups was its non-monotonic trend, with the highest vascular count recorded at 0.05 mg L⁻¹ after 48 hours, whereas the maximal response was noted at 0.5 mg L⁻¹ after 72 hours. Such dynamics likely reflect the interplay between early immune-driven angiogenesis and subsequent compensatory mechanisms. At lower doses and shorter times, neovascularisation may be rapidly induced as an adaptive attempt to restore tissue homeostasis and facilitate recruitment



of immune effectors. At later time points and higher concentrations, however, the progressive accumulation of PET NPs and ROS may exacerbate tissue stress, amplifying angiogenic signalling pathways, including those mediated by inflammatory cytokines and hypoxia-related factors. This biphasic or time-shifted behaviour is consistent with hormetic responses described in other invertebrate and vertebrate models, where initial moderate stress promotes repair mechanisms, but sustained or higher-level exposure further stimulates angiogenesis through pathological remodelling rather than adaptive compensation.³² In *H. verbana*, this may particularly involve remodelling of the botryoidal tissue, a hematopoietic-vascular niche highly sensitive to redox imbalance and inflammatory cues.

In parallel, oxidative stress emerged as a major downstream effect of PET NP exposure. Indeed, antioxidant enzymes, such as catalase (CAT), GST and SOD, are essential for defending cells from oxidative stress caused by microplastics and nanoplastics, as they help neutralise reactive oxygen species (ROS) and restore intracellular balance.³⁵ CAT and SOD's key role in counteracting plastic particles exposure adverse effects was already observed in other invertebrate models, including *C. elegans* and *D. melanogaster*, in which their activity was clearly enhanced.^{36,37} Similarly, GST gene expression in *Daphnia pulex* and *Eisenia foetida* showed a marked increase following nanoplastic exposure.^{38,39} This pattern was paralleled by an increase in ROS production measured by the H₂DCFDA assay, which revealed a significant elevation in intracellular ROS levels, particularly at high concentrations during short exposures. Over time, ROS levels tended to stabilise or decrease at the highest doses, likely reflecting cellular adaptation or exhaustion of the antioxidant response, consistent with the gene expression profiles observed. These findings support the role of oxidative stress as a key mechanism in the response of *H. verbana*⁴⁰ to xenobiotic exposure. Expression of antioxidant enzymes GST4A and SOD was significantly upregulated, showing a classic time- and dose-dependent trend: both genes peaked at high concentrations after short-term exposure, while after 1 month, maximal induction was observed at intermediate doses, again indicative of a biphasic response. This suggests that prolonged exposure to high NP concentrations may compromise the organism's antioxidant capacity, possibly due to enzyme depletion or cellular damage from excessive ROS accumulation. A more detailed understanding of this oxidative stress response reveals that the initial upregulation of antioxidant enzymes likely represents an effective attempt by the organism to counteract elevated ROS levels generated by PET NP exposure. However, with prolonged or high-dose exposure, these defence mechanisms may become overwhelmed, leading to diminished enzymatic activity through depletion or oxidative inactivation. This decline compromises the ability to neutralise.

ROS exacerbate cellular and tissue damage. The accumulation of ROS not only affects cellular components but can also trigger lipid peroxidation, protein oxidation, and DNA damage, potentially impairing cellular function and survival. In response, *H. verbana* appears to deploy compensatory

mechanisms such as increased mucus secretion, rich in glycoproteins and antioxidant molecules, which may form a biochemical barrier to limit nanoparticle penetration and oxidative harm. This dual strategy, enzymatic detoxification coupled with extracellular protective secretions, highlights a complex and dynamic physiological adaptation aimed at maintaining redox homeostasis and tissue integrity under nanoparticle-induced oxidative stress. These insights align with findings in other aquatic invertebrates, where similar antioxidant defences and mucus-mediated protective roles are crucial for survival under environmental pollutant exposure.^{41,42}

Notably, these findings mirror previous results in *H. verbana*¹² and in *Erpobdella johanssoni*,²² exposed respectively to polypropylene and polyethylene particles, where oxidative stress was accompanied by a significant increase in mucus-secreting epithelial cells, particularly those containing type II granules. This mucus, rich in glycoproteins and antioxidant molecules, likely contributes to both physical entrapment and chemical neutralisation of nanoparticles. Such a dual protective function of mucus has been described in various aquatic invertebrates, further supporting its role in adaptive stress responses.^{28,43}

Taken together, our findings demonstrate that *H. verbana* mounts a coordinated and evolutionarily conserved response to PET NP exposure, involving immune activation, redox regulation, and vascular remodelling. Acute exposures primarily trigger pro-inflammatory and angiogenic pathways, while chronic exposures highlight the limits of physiological compensation, with signs of immune suppression, oxidative imbalance, and tissue adaptation. These results reinforce the suitability of *H. verbana* as an *in vivo* model for evaluating nanoplastic toxicity and environmental pollutant effects in aquatic ecosystems, offering insight into dose- and time-dependent thresholds of biological resilience.

In addition, this biphasic pattern observed in leeches under chronic PET NP exposure raises important ecological concerns. Although the moderate activation of immune and antioxidant defences may initially enhance resilience, the subsequent decline at higher doses of nanoplastics suggests the onset of immune exhaustion and reduced oxidative buffering capacity. In natural ecosystems, such long-term immunosuppression could increase host susceptibility to pathogens, ultimately compromising the survival and reproductive output of organisms. At the population level, these effects may translate into altered demographic distributions and growth.^{44,45} A decline in the *H. verbana* population health and abundance could have significant effects on the trophic chain, weakening ecosystem stability and resilience. Similarly, biphasic trends have also been reported in other aquatic invertebrates exposed to pollutants, further suggesting that this response may represent a conserved but fragile adaptive strategy, which carries long-term ecological costs under sustained contaminant exposure.^{46,47} For all these reasons, the ecological consequences of chronic PET NP exposure warrant careful consideration. A decline both in the innate immune functions and in the fitness of benthic invertebrates such as leeches could disrupt predator-



prey and host–parasite interactions, altering community composition and impairing many ecosystem functions, including nutrient cycling and organic matter decomposition. Over time, such disruptions may reduce biodiversity and compromise the resilience of freshwater ecosystems to additional stressors. These findings thus emphasise the importance of integrating nanoplastic contamination into ecological risk assessments and highlight the broader environmental significance of the responses observed in this model organism.

Future studies will focus on the impact of PET nanoplastics on regenerative processes in *H. verbana*, with particular attention to how chronic exposure may impair tissue renewal and post-injury repair, thus providing a more comprehensive understanding of the long-term ecological risks associated with nanoparticle contamination.

Conclusions

This study provides a comprehensive overview of the inflammatory and immunological responses triggered by PET NPs in *H. verbana*. The findings highlight how this pollutant is able to induce the activation of well-conserved stress and defence pathways. Inflammatory and oxidative stress activation were shown to be strictly linked to increased concentration of NPs in a dose and time-dependent manner, despite showing limitations in long-term exposure. The observed biphasic pattern is indeed representative of the disruptive and unbalancing effect that PET NPs may exert on living organisms when constitutively exposed to high concentrations of pollutants, drawing more focus and the possible threatening consequences of plastic contamination. Overall, these results confirm *H. verbana* as a sensible model for ecotoxicological studies in freshwater environments, establishing a basis for future studies investigating nanoparticles effects on physiological mechanisms involved in immune response and regeneration events.

Author contributions

C. B.: formal analysis, investigation, writing – review and editing. L. P.: formal analysis, investigation, validation, writing – review and editing. E. B.: formal analysis, investigation, writing – review and editing. S. A.: formal analysis, investigation, writing – review and editing. M. B.: formal analysis, investigation, writing – review and editing. D. T.: formal analysis, methodology, supervision; writing – review and editing. N. B.: formal analysis, funding acquisition, supervision; validation; writing – original draft. A. G.: conceptualization, funding acquisition, project administration, supervision, validation, writing – original draft.

Conflicts of interest

The authors declare no conflicts of interest.

Data availability

All data generated or analyzed during this study are included in this article and its supplementary information (SI).

Supplementary information: content of SI: 1. List of mean values and 95% confidence intervals for: vessel counts, CD31 expression, ACP-positive cells, and gene expression of *HmAIF-1*, *SOD*, and *GST*. 2. DLS analyses on non-fluorescent PET NPs. 3. Immunofluorescence negative controls. 4. ROS detection using fluorescence dye 2',7'-dichlorodihydrofluorescein diacetate (H_2DCFDA). See DOI: <https://doi.org/10.1039/d5en00733j>.

Acknowledgements

This research was funded by PRIN (Progetti di Ricerca di rilevante Interesse Nazionale), grant number 2022SAHTRX by A. G. and by FAR (Fondo di Ateneo per la Ricerca) by A. G. and N. B. C. B. is a PhD student of Life Sciences and Biotechnology course at University of Insubria. Scientific support from CRIETT center of University of Insubria (instrument code MIC01) is greatly acknowledged.

References

- O. Pencik, K. Molnarova, M. Durdakova, M. Kolackova, D. Klofac and A. Kucsera, *et al.*, Not so dangerous? PET microplastics toxicity on freshwater microalgae and cyanobacteria, *Environ. Pollut.*, 2023, **329**, 121628, available from: <https://www.sciencedirect.com/science/article/pii/S0269749123006309>.
- X. Shi, Z. Chen, W. Wei and B. J. Ni, Perspectives on sustainable plastic treatment: A shift from linear to circular economy, *TrAC, Trends Anal. Chem.*, 2024, **173**, 117631, available from: <https://www.sciencedirect.com/science/article/pii/S0165993624001134>.
- G. Oliveri Conti, P. Rapisarda and M. Ferrante, Relationship between climate change and environmental microplastics: a one health vision for the platysphere health, *One Health Adv.*, 2024, **2**(1), 17, DOI: [10.1186/s44280-024-00049-9](https://doi.org/10.1186/s44280-024-00049-9).
- D. Magri, M. Veronesi, P. Sánchez-Moreno, V. Tolardo, T. Bandiera and P. P. Pompa, *et al.*, PET nanoplastics interactions with water contaminants and their impact on human cells, *Environ. Pollut.*, 2021, **271**, 116262, available from: <https://pubmed.ncbi.nlm.nih.gov/33360657/>.
- S. Ducoli, S. Federici, M. Cocca, G. Gentile, A. Zandrini and P. Bergese, *et al.*, Characterization of polyethylene terephthalate (PET) and polyamide (PA) true-to-life nanoplastics and their biological interactions, *Environ. Pollut.*, 2024, **343**, 123150, available from: <https://pubmed.ncbi.nlm.nih.gov/38103711/>.
- K. Bodó, N. Baranzini, R. Girardello, B. Kokhanyuk, P. Németh and Y. Hayashi, *et al.*, Nanomaterials and annelid immunity: A comparative survey to reveal the common stress and defense responses of two sentinel species to nanomaterials in the environment, *Biology*, 2020, **9**(10), 307, DOI: [10.3390/biology9100307](https://doi.org/10.3390/biology9100307).



- 7 J. M. Gonçalves, V. S. Sousa, M. R. Teixeira and M. J. Bebianno, Chronic toxicity of polystyrene nanoparticles in the marine mussel *Mytilus galloprovincialis*, *Chemosphere*, 2022, **287**(Pt 4), 132356, available from: <https://pubmed.ncbi.nlm.nih.gov/34600009/>.
- 8 M. Esterhuizen, M. Monticelli, S. A. Lee, Y. Kim, S. Pflugmacher and Y. J. Kim, Oxidative stress status and antioxidative responses in neonate versus adult *Daphnia magna* exposed to polystyrene leachate, *J. Toxicol. Environ. Health Sci.*, 2024, **16**, 171–179, DOI: [10.1007/s13530-024-00211-1](https://doi.org/10.1007/s13530-024-00211-1).
- 9 A. Grimaldi, G. Tettamanti, G. Perletti, R. Valvassori and M. De Eguileor, Hematopoietic Cell Formation in Leech Wound Healing, *Curr. Pharm. Des.*, 2006, **12**(24), 3033–3041, DOI: [10.2174/138161206777947443](https://doi.org/10.2174/138161206777947443).
- 10 R. T. Sawyer, *Leech Biology and Behaviour*, Oxford Science Publications, 1986, available from: <https://www.biopharm-leeches.com>.
- 11 E. R. Macagno, T. Gaasterland, L. Edsall, V. Bafna, M. B. Soares and T. Scheetz, *et al.*, Construction of a medicinal leech transcriptome database and its application to the identification of leech homologs of neural and innate immune genes, *BMC Genomics*, 2010, **11**, 407, available from: <https://www.biomedcentral.com/1471-2164/11/407>.
- 12 N. Baranzini, L. Pulze, C. Bon, L. Izzo, S. Pragliola and V. Venditto, *et al.*, *Hirudo verbana* as a freshwater invertebrate model to assess the effects of polypropylene micro and nanoplastics dispersion in freshwater, *Fish Shellfish Immunol.*, 2022, **127**, 492–507, DOI: [10.1016/j.fsi.2022.06.043](https://doi.org/10.1016/j.fsi.2022.06.043).
- 13 A. Calisi, N. Baranzini, G. Marcolli, C. Bon, D. Rotondo and D. Gualandris, *et al.*, Evaluation of per- and polyfluoroalkyl substances (PFAS) toxic effects on the acute inflammatory response in the medicinal leech *Hirudo verbana*, *Chemosphere*, 2024, **366**, 143519, DOI: [10.1016/j.chemosphere.2024.143519](https://doi.org/10.1016/j.chemosphere.2024.143519).
- 14 A. Grimaldi, G. Tettamanti and M. de Eguileor, Annelida: Hirudinea (Leeches): Heterogeneity in Leech Immune Responses, *Advances in Comparative Immunology*, 2018, 173–191, DOI: [10.1007/978-3-319-76768-0_8](https://doi.org/10.1007/978-3-319-76768-0_8).
- 15 N. Rajtar, M. Starek, L. Vincenti, M. Dąbrowska, M. Romek and R. Rinaldi, *et al.*, Effect of PET Micro/Nanoplastics on Model Freshwater Zooplankton, *Polymers*, 2025, **17**(9), 1256, available from: <https://www.mdpi.com/2073-4360/17/9/1256/htm>.
- 16 C. Jiang, L. Yin, Z. Li, X. Wen, X. Luo and S. Hu, *et al.*, Microplastic pollution in the rivers of the Tibet Plateau, *Environ. Pollut.*, 2019, **249**, 91–98, available from: <https://www.sciencedirect.com/science/article/pii/S0269749118349182>.
- 17 K. Pelegrini, T. C. B. Pereira, C. C. S. Wertheimer, L. De Souza Teodoro, N. R. De Souza Basso and R. A. Ligabue, *et al.*, Microplastics Beach Pollution: Composition, Quantification and Distribution on the Southern Coast of Brazil, *Water, Air, Soil Pollut.*, 2024, **235**(11), 1–21, DOI: [10.1007/s11270-024-07541-3](https://doi.org/10.1007/s11270-024-07541-3).
- 18 V. Pirillo, L. Pollegioni and G. Molla, Analytical methods for the investigation of enzyme-catalyzed degradation of polyethylene terephthalate, *FEBS J.*, 2021, **288**(16), 4730–4745, DOI: [10.1111/febs.15850](https://doi.org/10.1111/febs.15850).
- 19 A. Grimaldi, S. Banfi, L. Gerosa, G. Tettamanti, D. M. Noonan and R. Valvassori, *et al.*, Identification, Isolation and Expansion of Myoendothelial Cells Involved in Leech Muscle Regeneration, *PLoS One*, 2009, **4**(10), e7652, available from: <https://journals.plos.org/plosone/article?id=10.1371/journal.pone.0007652>.
- 20 F. Drago, P. E. Sautière, F. Le Marrec-Croq, A. Accorsi, C. Van Camp and M. Salzet, *et al.*, Microglia of medicinal leech (*Hirudo medicinalis*) express a specific activation marker homologous to vertebrate ionized calcium-binding adapter molecule 1 (Iba1/alias aif-1), *Dev. Neurobiol.*, 2014, **74**(10), 987–1001, DOI: [10.1002/dneu.22179](https://doi.org/10.1002/dneu.22179).
- 21 T. Schorn, F. Drago, M. De Eguileor, R. Valvassori, J. Vizioli and G. Tettamanti, *et al.*, The Allograft Inflammatory Factor-1 (AIF-1) homologous in *Hirudo medicinalis* (medicinal leech) is involved in immune response during wound healing and graft rejection processes, *Invertebrate Surviv. J.*, 2015, **12**, 129–141.
- 22 R. Ben Ahmed, I. Khaled, T. El Ayari, I. Saidi and A. H. Harrath, Assessing the Effect of Polyethylene Microplastics in the Freshwater Leech *Erpobdella johanssoni* (Annelida, Hirudinida) Through Integrated Biomarkers and Histopathological Analysis, *Animals*, 2025, **15**(10), 1417, available from: <https://www.mdpi.com/2076-2615/15/10/1417/htm>.
- 23 C. Gambardella, S. Morgana, M. Bramini, A. Rotini, L. Manfra and L. Migliore, *et al.*, Ecotoxicological effects of polystyrene microbeads in a battery of marine organisms belonging to different trophic levels, *Mar. Environ. Res.*, 2018, **141**, 313–321, available from: https://www.sciencedirect.com/science/article/pii/S0141113618301533?casa_token=ia0dpzvtoGYAAAAA:OKfFL-mxB545S2qUb5YUWHTA9o53V4O8G_Dw7YfQ2yb-u25HvOQ-BBGRcXwBeWqH356MJfW4Vk.
- 24 X. Wang, S. Shao, T. Zhang, Q. Zhang, D. Yang and J. Zhao, Effects of exposure to nanoplastics on the gill of mussels *Mytilus galloprovincialis*: An integrated perspective from multiple biomarkers, *Mar. Environ. Res.*, 2023, **191**, 106174, available from: <https://pubmed.ncbi.nlm.nih.gov/37708618/>.
- 25 M. Sendra, E. Sparaventi, B. Novoa and A. Figueras, An overview of the internalization and effects of microplastics and nanoplastics as pollutants of emerging concern in bivalves, *Sci. Total Environ.*, 2021, **753**, 142024, available from: https://www.sciencedirect.com/science/article/pii/S0048969720355534?casa_token=C6MsHZIJTPcAAAAA:jE3LCO_6Mh5cOTeoGEkHiTvRBFuWsj_7JD9vVWMQt-XyQxMpnUjgQEvPCz7yYiW6u5Oafi_d55U.
- 26 J. Bhagat, L. Zang, N. Nishimura and Y. Shimada, Zebrafish: An emerging model to study microplastic and nanoplastic toxicity, *Sci. Total Environ.*, 2020, **728**, 138707, available from: https://www.sciencedirect.com/science/article/pii/S0048969720322245?casa_token=3U0PTjzJLG4AAAAA:



- [LDB0emfF6S1-PhdIaPhCUlCmGQ9XTUy2q-YAPBGjRZw0jFq7BNAtdOa6sTNhV4G3XDxeP7erKMI.](#)
- 27 M. Cole, P. Lindeque, E. Fileman, C. Halsband and T. S. Galloway, The impact of polystyrene microplastics on feeding, function and fecundity in the marine copepod *Calanus helgolandicus*, *Environ. Sci. Technol.*, 2015, **49**(2), 1130–1137, DOI: [10.1021/es504525u?ref=article_openPDF](#).
- 28 N. T. Q. Mai, U. Batjargal, W. S. Kim, J. H. Kim, J. W. Park and I. S. Kwak, *et al.*, Microplastic induces mitochondrial pathway mediated cellular apoptosis in mussel (*Mytilus galloprovincialis*) via inhibition of the AKT and ERK signaling pathway, *Cell Death Discovery*, 2023, **9**(1), 442, available from: <https://pmc.ncbi.nlm.nih.gov/articles/PMC10700607/>.
- 29 T. Lajqi, N. Köstlin-Gille, R. Bauer, S. G. Zarogiannis, E. Lajqi and V. Ajeti, *et al.*, Training vs. Tolerance: The Yin/Yang of the Innate Immune System, *Biomedicines*, 2023, **11**(3), 766, available from: <https://www.mdpi.com/2227-9059/11/3/766/htm>.
- 30 M. Auguste, T. Balbi, C. Ciacci, B. Canonico, S. Papa and A. Borello, *et al.*, Shift in Immune Parameters After Repeated Exposure to Nanoplastics in the Marine Bivalve *Mytilus*, *Front. Immunol.*, 2020, **11**, 426, available from: <https://www.frontiersin.org/journals/immunology/articles/10.3389/fimmu.2020.00426/full>.
- 31 C. Huang, X. Feng, S. Yue, L. Jia, K. Wang and W. Zhou, *et al.*, Impact of progressively cumulative exposure of AgNPs on earthworms (*Eisenia fetida*) and implication for ecotoxicological risk assessment, *Chemosphere*, 2023, **322**, 138163, available from: https://www.sciencedirect.com/science/article/pii/S0045653523004307?casa_token=IING-bD8z-gAAAAA:5xy3fuO4-vNL3067UPlhxZPC_AUAM_bWtgZnhKADIsLYqgrhiGXiZ8uDHYKrGfdnPKPYdh7HIIM.
- 32 T. Lajqi, N. Köstlin-Gille, R. Bauer, S. G. Zarogiannis, E. Lajqi and V. Ajeti, *et al.*, Training vs. tolerance: the Yin/Yang of the innate immune system, *Biomedicines*, 2023, **11**(3), 766, available from: <https://www.mdpi.com/2227-9059/11/3/766>.
- 33 T. A. Gorr, M. Gassmann and P. Wappner, Sensing and responding to hypoxia via HIF in model invertebrates, *J. Insect Physiol.*, 2006, **52**(4), 349–364, available from: https://www.sciencedirect.com/science/article/pii/S0022191006000060?casa_token=WPuy5mICaXQAAAAA:R0XHLJRyLaBFc7DDQyrA4s8tLU9e8r5mfF9l3idrrrhvaCIGYGWO-lV2B0oKh-ARHo2vxeo1ds0.
- 34 A. Graham and F. S. Barreto, Independent losses of the hypoxia-inducible factor (HIF) pathway within Crustacea, *Mol. Biol. Evol.*, 2020, **37**(5), 1342–1349, available from: <https://academic.oup.com/mbe/article-abstract/37/5/1342/5719058>.
- 35 A. Das, The emerging role of microplastics in systemic toxicity: Involvement of reactive oxygen species (ROS), *Sci. Total Environ.*, 2023, **895**, 165076, available from: https://www.sciencedirect.com/science/article/pii/S0048969723036999?casa_token=EWQ0cBd4pm4AAAAA:B1RQ2mCuLiQoqRwNvNngY6gk-4FSVbdQGg6HInorDegl1HZzZO8GFoJcsCavEWWtNg_GheC3KUg.
- 36 J. Chen, C. Chen, Z. Luo, X. Jin, Y. Chen and Q. Wu, *et al.*, The role of Sod-2 in different types of neuronal damage and behavioral changes induced by polystyrene nanoplastics in *Caenorhabditis elegans*, *Ecotoxicol. Environ. Saf.*, 2024, **288**, 117416, available from: <https://www.sciencedirect.com/science/article/pii/S0147651324014921>.
- 37 S. Bauri, H. Shekhar, H. Sahoo and M. Mishra, Investigation of the effects of nanoplastic polyethylene terephthalate on environmental toxicology using model *Drosophila melanogaster*, *Nanotoxicology*, 2024, **18**(4), 354–372, DOI: [10.1080/17435390.2024.2368004](#).
- 38 Z. Liu, Y. Zhang, Y. Zheng, Y. Feng, W. Zhang and S. Gong, *et al.*, Genome-wide identification glutathione-S-transferase gene superfamily in *Daphnia pulex* and its transcriptional response to nanoplastics, *Int. J. Biol. Macromol.*, 2023, **230**, 123112, available from: <https://pubmed.ncbi.nlm.nih.gov/36621743/>.
- 39 Y. Zhou, G. He, H. Jiang, K. Pan and W. Liu, Nanoplastics induces oxidative stress and triggers lysosome-associated immune-defensive cell death in the earthworm *Eisenia fetida*, *Environ. Int.*, 2023, **174**, 107899, available from: <https://www.sciencedirect.com/science/article/pii/S0160412023001721>.
- 40 R. Girardello, N. Baranzini, G. Tettamanti, M. De Eguileor and A. Grimaldi, Cellular responses induced by multi-walled carbon nanotubes: in vivo and in vitro studies on the medicinal leech macrophages, *Sci. Rep.*, 2017, **7**(1), 8871, available from: <https://pubmed.ncbi.nlm.nih.gov/28827736/>.
- 41 J. Li, K. Yin, L. Hou, Y. Zhang, H. Lu and C. Ma, *et al.*, Polystyrene microplastics mediate inflammatory responses in the chicken thymus by Nrf2/NF- κ B pathway and trigger autophagy and apoptosis, *Environ. Toxicol. Pharmacol.*, 2023, **100**, 104136, available from: <https://pubmed.ncbi.nlm.nih.gov/37127111/>.
- 42 X. Wang, M. Gao, X. Lu, Y. Lei, J. Sun and M. Ren, *et al.*, Resveratrol alleviates Mono-2-ethylhexyl phthalate-induced mitophagy, ferroptosis, and immunological dysfunction in grass carp hepatocytes by regulating the Nrf2 pathway, *J. Environ. Manage.*, 2024, **371**, 123235, available from: <https://pubmed.ncbi.nlm.nih.gov/39509968/>.
- 43 A. Sinha, V. Matey, T. Giblen, R. Blust and G. De Boeck, Gill remodeling in three freshwater teleosts in response to high environmental ammonia, *Aquat. Toxicol.*, 2014, **155**, 166–180, available from: https://www.sciencedirect.com/science/article/pii/S0166445X14002318?casa_token=RSZ3WHtbyeEAAAAA:C7JGjpfne8VEmk-4qOJdedFw-Ng8TWN6lnoAZ-9mTOcOO7YutWYD6M2Wd0Z3hjy4VtUEJvuE.
- 44 C. Kataoka and S. Kashiwada, Ecological Risks Due to Immunotoxicological Effects on Aquatic Organisms, *Int. J. Mol. Sci.*, 2021, **22**(15), 8305, available from: <https://www.mdpi.com/1422-0067/22/15/8305/htm>.
- 45 Z. Abdul Kari, Abiotic and biotic factors affecting the immune system of aquatic species: A review, *Comp Immunol Rep.*, 2025, **9**, 200230, available from: <https://www.sciencedirect.com/science/article/pii/S2950311625000369?via%3Dihub>.



- 46 E. Agathokleous, E. J. Calabrese and D. Barceló, Environmental hormesis: New developments, *Sci. Total Environ.*, 2024, **906**, 167450, available from: <https://www.sciencedirect.com/science/article/abs/pii/S0048969723060771?via%3Dihub>.
- 47 R. Berry and G. López-Martínez, A dose of experimental hormesis: When mild stress protects and improves animal performance, *Comp. Biochem. Physiol., Part A: Mol. Integr. Physiol.*, 2020, **242**, 110658, available from: <https://www.sciencedirect.com/science/article/pii/S1095643320300106?via%3Dihub>.

